ISSN: 2791-9293 Volume: 2 Issue: 2 Year: 2022

JOMCOM

Journal of Millimeterwave Communication, Optimization and Modelling

editor in chief

Assoc. Prof. M. Tahir GUNESER

CONTENT

Content i

About the Journal ii

Editor in Chief ii

Publisher ii

Aims & Scope iii

1. Modeling and Simulation of a Doubly Fed Induction Generator Based Wind Turbine

Khalid Waleed Nasser *69-76*

2. Optimal Power Flow by using Distributed Generation in Six Buses Iraqi Network

Husham Sulaiman Sajir *77-81*

3. Techno-Economic Analysis of Grid-Connected PV Systems Using BAT Algorithms and Comparison with other Algorithms

Abdurazaq Elbaz *82-88*

4. Performance Analysis Rectangular Patch Antenna 3.5 GHz for Wi-Max and WLAN

Ali Abozied, Abdelaziz Al-dawi, Cihat Seker *89-93*

5. Simulation of Rectangular Microstrip Antennas and the Effect of Variable Frequencies and Performance Analysis

Ali Abozied *94-97*

About the Journal

Journal of Millimeterwave Communication, Optimization and Modelling (JOMCOM) is an international on-line and refereed journal published 2 times a year (June and December) in English. Journal of Millimeterwave Communication, Optimization and Modelling (JOMCOM) published its first issue in 2021 and has been publishing since 2021. Manuscripts in JOMCOM Journal reviewed of at least 2 referees among the referees who have at least doctorate level in their field.

Journal of Millimeterwave Communication, Optimization and Modelling (JOMCOM) is an international online journal that is published 2 times in a year in English.

The purpose of JOMCOM is publishing the scientific research in various fields of communication.

All kinds of transactions and the application about the journal can be made from **https://jomcom.org**

The scientific responsibility of articles belongs to the authors.

ISSN: 2791-9293

Editor in Chief:

Assoc. Prof. Dr. Muhammet Tahir GÜNEŞER

Karabük University

Faculty of Engineering

Department of Electrical and Electronics Engineering

Head of Communication Division

Karabük, TURKEY

jomcomeditor@gmail.com

PUBLISHER

Assoc. Prof. Muhammet Tahir GÜNEŞER

Aims & Scope

Communication Technologies: Journal of Millimeter-wave Communication, Optimization and Modelling (JOMCOM) publishes original research and review articles in Communication Technologies, Innovative Technologies, and Systems in the broad field of Information-Communication Technology. Purpose of JOMCOM; To create value in the field by publishing original studies that will contribute to the literature in wireless communication sciences and be a resource for academia and industrial application whole over the world. Besides, JOMCOM aims to bring the valuable work of researchers working in Communication studies to a broader audience at home and abroad. Readership of JOMCOM; valuable representatives of the wireless communication area, especially those who do academic studies in it, and those who do academic studies about modelling and system design and other interested parties. Since JOMCOM will appeal to a broader audience in article submissions, it prioritizes studies prepared in English.

Optimization and Modelling: Journal of Millimeter-wave Communication, Optimization and Modelling (JOMCOM), within the scope of Wireless Communication Sciences, publishes articles on communication theory and techniques, systems and networks, applications, development and regulatory policies, standards, and management techniques. It also reports experiences and experiments, best practices and solutions, lessons learned, and case studies. Additional studies on System Design, Modelling and Optimization. Subject areas of interest covered in the journal include the following but are not limited to:

5G-6G Technologies

Circuits for Optical Communication Systems

Antenna Design

Communication Design Materials

Fiber Optic Communication

Innovative Designs for Communications

Integrated Circuits for Communications

Optimization Methods on Engineering

Realization of Antenna Systems

Realization of Microwave, Radar, and Sonar Systems

RF Circuits

System Design

Visible Light Communication

Wireless Communication

Modeling and Simulation of a Doubly Fed Induction Generator Based Wind Turbine

Received: 8 June 2022; Revised: 11 August 2022;
Accepted: 25 December 2022

Research Article

Khalid Waleed Nasser
Department of electrical engineering
University of Misan
Misan, Iraq
khalid.waleed@uomisan.edu.iq
ORCID: 0000-0002-2384-7031

***Abstract*— Wind power's fundamental difficulties are becoming more visible as the system's penetration grows. Wind energy fluctuation must be reduced, and large-scale units must be connected to the grid constantly and dependably. Despite conventional power vector control can achieve decoupling control, DFIG has a high reliance on elements; therefore power control and maximum power tracing is a critical area of research. The DFIG model is constructed on the MATLAB/Simulink platform and is based on an examination of active power research's current state. The impact of wind speed on power generated, pitch angle, and reactive power is investigated by simulating the dynamic model of a DFIG WT.**

Keywords—DFIG, wind turbine, doubly fed induction generator,

I. INTRODUCTION

The environment is concerned about the global energy crisis and climate change. Renewable sources of energy have developed as a new model for meeting our society's energy needs. Hydroelectric power, solar, wind, geothermal heat, tides, seas, and biofuel energy supplies have all attracted much attention in recent years. The future of the power sector will be characterized by wind energy. Wind power generation technologies have attracted widespread attention due to their fast development . DFIGs have several advantages in modern energy systems, including operation at varied speeds and real and reactive power characteristics. The stator is connected to the electricity grid directly in DFIG. In contrast, the rotor is connected via a bi-directional converter to regulate active and reactive power among the stator and the alternative current system [1]. The rotor flow is based on wind turbine technology and disconcerts the vector control approach into active and reactive power elements. Rotor current control systems regulate these elements by rectifying the rotor current excitation voltage [2, 3]. The issues should be overcome for massive wind farm operations. The electromechanical model created a nonlinear feedback controller by coupling DFIG with turbines for wind. The increased utilized of replenishable energy is mandated on a global scale owing to traditional power plants' energy key pollution and non-sustainability [4]. Many technical problems involving systems of electricity, such as voltage stability, reliability, and protection. Wind energy is gaining popularity as a sustainable energy source that is less expensive than traditional electricity sources. Wind energy is erratic due to substantial changes in the natural wind. Due to considerable insignificant changes compared to conventional energy sources, the wind energy conversion system confronts major hurdles [5]. The power outage variation generates variation in frequency, implying the unsteadiness of a high penetration system. Because of the large variability in output power, wind energy conversion devices are considered hazardous loads [6]. The transmission of nonlinearity of wind farms owing to the DFIG physical model is affected by wind swiftness and rotation of electro-magnetic torque. For both stator and rotor current flow are nonlinear functions. The rotor current controller must be carefully tuned to maintain the steadiness of the closed-loop technique and adequate transient reaction into the working scope [7, 8]. As well, vector control demands flux prediction or mensuration. It is essential to move up and down to generate units to satisfy active and reactive power requirements [3]. The accompanying preservation expense of such manipulation activities ought kept low, as must the network's requirement for wind turbines to ride through the ability of external AC disruption. An enhanced control in the presence of an imbalanced voltage and enhances the fluctuation in grid voltage is suggested for controlling the overcurrent of the generator by keeping an eye on the network failure [9]. The investigation of the fault current characteristics of DFIGs is a prerequisite for fixing the difficulties of relaying electrical system's protection with DFIGs. These criteria vary from those of a traditional synchronous generator. Under different settings, the fault current properties of DFIG (damping temporal constants as well as transient elements) are variable. As a result, the research of DFIG features for specific situations is required [2, 10-12]. For fault circumstances, numerous research has been recommended. However, due to the intricate consequences of the dynamic reaction of an AC/DC/AC converter according to fault situations, analyzing the current fault characteristics of the DFIG is hugely challenging. The DFIG fault current was investigated on the assumption that the excitation current would be fixed before and after the fault occurred [11-14]. The research is unsuitable for practical systems because it is based on the stated assumption. As other high-quality, research was conducted for properties of fault current while taking in consideration the rotor side converter (RSC) and grid side converter's dynamic response (GSC). The work offered in that study is insufficient to fulfill the criteria of the relaying protection study. To close this gap, a theoretical, analytical approach for the DFIG The characteristic of fault current in non-severe conditions is proposed. The rotor windings are still excited, and the dynamic reaction significantly impacts the stator fault current characteristics. Wind turbines must be integrated and participate actively in maintaining system stability during and after disruptions or failures. Other system dynamics could deteriorate as a result of this strategy. In the

sector of transient investigations, the disruption of the field is separated from the turbine generator's way of behaving [8, 15]. The boundary of the rotor side converter can raise the stator fault current and DC link voltage to achieve the DFIG needs through the voltage dip. The theoretical underpinning of the inquiry was conducted, and the DFIG transient behavior enhanced after the disturbance in the study was removed. The dynamic model analysis was employed in the nonlinear control architecture to settle the nature of the instability and enhance the generator's performance [16].

II. LITERATURE SURVEY

H. Abouobaida: A control method for a grid connected (DFIG)-based WECS is presented in this research. Control algorithms for the DFIG's grid and rotor side converters, as well as simulation techniques of the design, are described. The established methodology control is simulated in MATLAB-SIMULINK, with the findings given at the conclusion of this study [1]. Adavipalli Chandanaet al., In relation to other renewable energy sources, wind turbines are more expensive. DFIG with Fuel Cells could be used to keep the active power at a consistent level. The power transfer matrix is a fresh idea for governing the DFIG introduced in this study. A matrix converter mechanism-based power/current controller is designed with the goal of protecting the DFIG during malfunctioning situations [4]. NihelKhemiri et al, The design and control concepts for a variable-speed constant-frequency WECS using a (DFIG) are discussed in this research paper. The wind energy converter system performed well under common wind variations, according to simulation findings generated with Matlab/Simulink. A backstepping control scheme is first constructed for the rotor side converter. A backstepping control system was originally created for the (RSC).The GSC is controlled using the same principles [17]. HU Jia-bing et al., A proportional-resonant (P-R) current control scheme and suitable control strategies for (GSC and RSC) are investigated for better control and fully operational of WECS that rely on DFIGs during voltage profile unbalancing circumstances. A P-R current control technique that is applied in the two-phase stator stationary reference for the DFIG's RSC when the system voltage is mismatched was introduced in this academic research with the goal of concurrently controlling the positive and negative sequence rotor currents using no sequential-decomposition method. Baseline calculations of positive and negative sequence rotor currents were shortened according to distinct enhanced control aims based on the positive-sequence d+-axis line voltage direction.

The P-R current controller's feasibility was validated by developing and building the appropriate control method for a DFIG wind power generating system under network instability. The results show that the recently developed P-R current controller can execute the RSC's control aims with an exceptional transient response. As a result, the DFIG wind generating system's ride-through capabilities have increased during unbalanced network fault conditions [18]. Jiabing Hu et al., The electromagnetic stability issues with grid-connected DFIG systems are frequently overlooked. This research offers a reduced-order small-signal model that may be used to examine the stability of DFIG's dc-link voltage controller, especially when the ac grid is not performing well. The DFIG flux and quick current control characteristics are ignored in this model. However, the effects of operating points, grid strength, and control loop interactions just on dynamic system performance are considered.

A comparison of eigenvalues shows that the suggested model demonstrates the dominant oscillation mode indicated by the detailed model, which is suitable for the stability study of the DFIG's dc-link voltage management system. Control loop interactions are also depicted using influence coefficients.

The recently launched model's application studies reveal that it is useful for demonstrating the effect of grid strength on the dynamic response of the DFIGs dc-link voltage controller. At the same moment, the effects of active power control (APC)/reactive power controls (RPC) on phase-locked loop (PLL) and rotor-side converter (RSC) stability of the system are explored [19]. P.GAYATHRI et al., The use of fuel has increased in tandem with the rise in worldwide power demand, harming the environment, and inspiring the use of renewable energy supplies.

The wind energy system is the most widely used and meets all power requirements. The DFIG is used in the proposed system for wind energy conversion, as well as harmonics scaling down and frequency management. When two back-to-back coupled Voltage Source Converters (VSCs) are retained between the rotor and the grid in DFIG, the stator is directly connected to the grid. Since the suggested DFIG operates as an active filter and generates active power in the same way as a typical DFIG, nonlinear loads are connected at PCC.

The PCC voltage is distorted due to harmonics created by the nonlinear load connected at the PCC. GSC control improves the nonlinear load harmonic currents to the point where the stator and grid currents are harmonic-free. Using a voltage-oriented reference frame, RSC is adjusted to achieve MPPT and also to achieve unity power factor at the stator side. For GSC control, a synchronous reference frame (SRF) control method is used to extract the basic component of load currents. Furthermore, PLL is used to monitor and modulate frequency. The MATLAB Simulink software is used to evaluate this newly presented technology.

III. GENERATING SYSTEM IN GENERAL

Figure 1 shows a structured methodology for generating electrical energy from wind power using a doubly-fed induction generator. The stator is fed to the network straight, whereas the rotor is plugged via a back-to-back converter [15]. The grid side converter is a PWM inverter, whereas the rotor side converter is a current regulate-voltage source inverter [20].

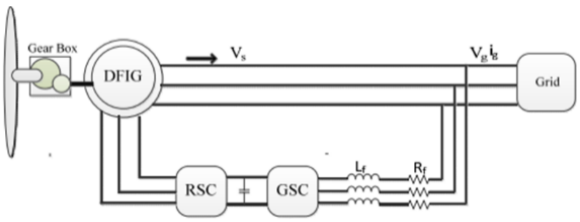

Fig. 1. Wind energy schematic diagram based on the DFIG system

A. Wind Turbine Pattern

The mechanical power caught by a wind turbine is as described in the following:

$$P_m = \frac{1}{2} C_p(\lambda, \beta) \rho R_T^2 \pi v V_\omega^3 \quad (1)$$

Where ρ reflects the density of the air, R_T the wind turbine radius, V_ω the wind speed, and C_p the wind turbine power coefficient. The C_p is calculated by:

$$C_p(\lambda, \beta) = 0.22\left(\frac{116}{\lambda_i} - 0.4\,\beta\text{-}5\right) e^{\frac{-12.5}{\lambda_i}} \quad (2)$$

$$\frac{1}{\lambda_i} = \frac{1}{\lambda + 0.08\,\beta} - \frac{0.035}{\beta^3 + 1} \quad (3)$$

where β symbolizes the blade pitch angle and λ symbolizes the tip speed ratio as described [10].

$$\lambda_{opt} = \frac{\omega_r R_T}{V_\omega} \quad (4)$$

Because of the existence of a gearbox with the gear ratio, the dynamic model wind turbine rotational speed ω_{rot} is related with the rotor speed ω_r:

$$\omega_r = n_g \lambda_{opt} \quad (5)$$

The exact dynamic model of the torque equation of the generator is given by,

$$T_m = \frac{P_m}{\omega_r} \quad (6)$$

It is a proportion of wind turbines that is measured, where Tm represents rotor torque and ωr denotes wind turbine velocity. Wind turbine speed affects the power coefficient. The theoretical maximum Cp is 0.59, although the actual range is 0.2-0.4 [21]. (4) and (5) yield the ideal generator speed for the optimum tip speed ratio:

$$\omega_r{}^{opt} = \frac{\lambda_{opt}\, n_g}{R_T} V_\omega \quad (7)$$

This refers to a high level of wind energy extraction P_m^{max} at the moment, the rotor torque of the generator can be calculated as:

$$T_m{}^{opt} = \frac{1}{2} \frac{\rho\, \pi\, R_T^5\, C_P^{opt}}{\lambda_{opt}^3} \omega_r{}^{opt} \quad (8)$$

The external input of the mechanical elements of the system is a wind turbine that rotates at the optimum rotational velocity and with the optimum torque of the nonlinear dynamic model of the doubly-fed induction generator.

B. The DFIG Model

The controller is often specified in a synchronous *d-q* frame that is linked to the stator voltage or flux [12, 22]. The generator dynamic model stated in a synchronously rotating frame *d-q* for the suggested control approach is:

$$\begin{aligned} V_{sd} &= R_s I_{sd} + \frac{d\emptyset_{sd}}{dt} - \omega_s . I_{sq} \\ V_{sq} &= R_s I_{sq} + \frac{d\emptyset_{sq}}{dt} - \omega_s . I_{sd} \\ V_{rd} &= R_r I_{rd} + \frac{d\emptyset_{rd}}{dt} - \omega_r . I_{rq} \\ V_{rq} &= R_r I_{rq} + \frac{d\emptyset_{rq}}{dt} - \omega_r . I_{rd} \end{aligned} \quad (9)$$

$$T_{em} = P\, M\, (I_{rd}\, I_{sq} - I_{rq}\, I_{sd}) \quad (10)$$

$$\begin{aligned} \emptyset_{sd} &= L_S\, I_{sd} + m . L_m\, I_{rd} \\ \emptyset_{sq} &= L_S\, I_{sq} + m . L_m\, I_{rq} \\ \emptyset_{rd} &= L_r\, I_{rd} + m . L_m\, I_{sd} \\ \emptyset_{rq} &= L_r\, I_{rq} + m . L_m\, I_{sq} \end{aligned} \quad (11)$$

Where V is the voltage, I is the current, $\emptyset$ is the flux, R is the resistance, L is the inductance, M is the mutual inductance, Tem is the electromagnetic torque, and P is the pole pair number. The following simplified model is adopted for the DFIG wind turbine:

$$\mathrm{J}\frac{\mathrm{d}\omega}{\mathrm{dt}} = \mathrm{T_m} - \mathrm{T_{em}} - \mathrm{K}.\,\omega \quad (12)$$

where $\mathrm{T_{em}}$ is the generator electromagnetic torque, J is the turbine total inertia, and K is the turbine total external damping. The stator and rotor powers, both real and reactive, are described by:

$$\begin{aligned} \mathrm{P_s} &= V_{sd}\, I_{sd} + V_{sq}\, I_{sq} \\ \mathrm{Q_s} &= V_{sq}\, I_{sd} - V_{sd}\, I_{sq} \\ \mathrm{P_r} &= V_{rd}\, I_{rd} + V_{rq}\, I_{rq} \\ \mathrm{Q_r} &= V_{rq}\, I_{rd} - V_{rq}\, I_{rq} \end{aligned} \quad (13)$$

Turbine speed is regulated as a function of wind speed to increase output power and increase system efficiency. Beyond a large power range, performance at maximum power could be accomplished. Common output power-speed lines as a result of turbine and wind speed are shown in Fig. 2 [5, 21].

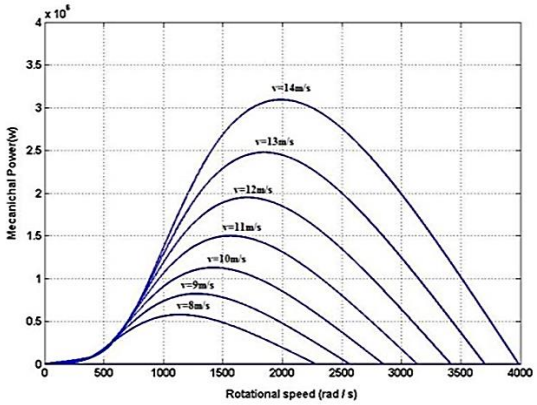

Fig. 2. Electrical output power as a function of turbine speed. Parameter curves are plotted for different wind speeds

C. Modeling of GSC and Grid

As shown in Fig. 3, this section focuses on the design of the AC/DC converter connected to the electrical grid through the RL filter.

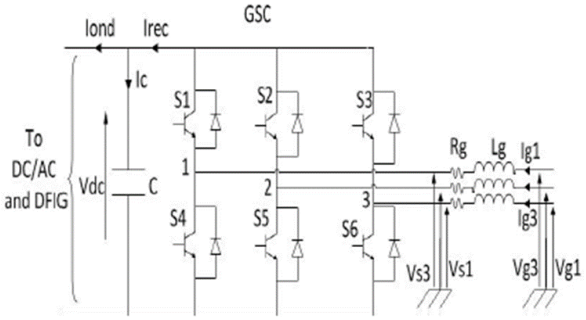

Fig. 3. Grid connected to AC/DC converter

The following equations represent the three-phase grid linked AC/DC converter design:

$$\begin{cases} \frac{CdVdc}{dt} = \text{Irec} - \text{Iond} \\ Vs1 = Vg1 - Rg \cdot Ig1 - Lg \cdot \frac{dIg\ 1}{dt} \\ Vs2 = Vg2 - Rg \cdot \text{Ig}\ 2 - Lg \cdot \frac{dIg\ 2}{dt} \\ Vs3 = Vg3 - Rg \cdot Ig3 - Lg \cdot \frac{dIg3}{dt} \end{cases} \quad (11)$$

With Vgi: electrical network voltages, Igi: electrical network currents, Irec, Iond: AC/DC converter output current and DC/AC converter input current, respectively. Vdc, Ic: the DC connection capacitor's voltage and current, respectively. Vsi: the AC/DC converter's input voltages IGBT transistor (Si).Control Methodology

Figure 4 depicts the controller's structure. It is based on a three-phase model of the wind system's electromechanical conversion chain [6]. Three goals guide the control method:

- "MPPT" is used to control the harvesting of peak wind power (Maximum PowerPoint Tracking),
- Controlling the RSC by adjusting the DFIG stator's electromagnetic torque and reactive power
- Controlling the DC bus voltage, active and reactive power shared with the network to regulate the GSC.

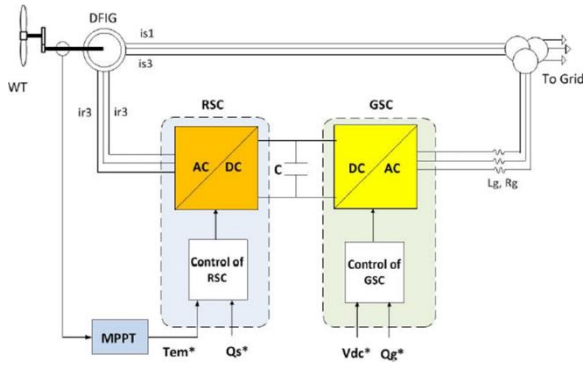

Fig. 4. Control strategy of wind energy conversion system

MPPT technique: Figure 5 illustrates the MPPT control theory for a wind turbine without controlling the rotation speed [12]. The control goal is to maximize wind energy harvesting by tracking the appropriate torque. *Tem**.

$$T_{em} *= k \cdot \omega_m^2 \quad (12)$$

With $$k = \frac{1}{2} \cdot \pi \cdot \rho \cdot R^5 \cdot \frac{Cp_{max}}{\lambda_{opt}^3}$$

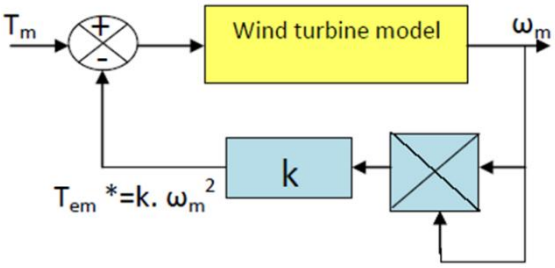

Fig. 5. MPPT control strategy

By adjusting the DFIG's dq-axes rotor currents, the electromagnetic torque and stator reactive power could be controlled. The stator field rotates at synchronous speed in a steady state. The stator flux vector represents this field and provides a visual representation of the phase and flux magnitude. We could construct by selecting the two-phase dq for the rotating stator field and positioning the stator flux vector on the d-axis. [14]:

$$\begin{cases} \Phi_s d = \Phi_s \\ \Phi_{sq} = 0 \end{cases} \quad (13)$$

By examining the selection of reference related to dq rotating stator field and eliminating the resistance of the stator windings, a modification of the DFIG formulas in the dq reference could be derived (9-11):

$$\begin{cases} V_{sq} = \omega_s \Phi_{sd}; V_{sd} = 0 \\ V_{rd} = R_r I_{rd} + \frac{d\Phi_{rd}}{dt} - \omega_r I_{rq} \\ V_{rq} = R_r I_{rq} + \frac{d\Phi_{rq}}{dt} + \omega_r I_{rd} \end{cases} \quad (14)$$

From the (9-11) of the stator and rotor flux in dq axes, the stator currents can be obtained from the following expressions:

$$\begin{cases} I_{sd} = \frac{\Phi_{sd} - m \cdot L_m \cdot I_{rd}}{L_s} \\ I_{sq} = \frac{m \cdot L_m}{L_s} \cdot I_{rq} \end{cases} \quad (15)$$

These expressions are then substituted into the (9-11) of the rotor flux which then become:

$$\begin{cases} \Phi_{rd} = \left(L_r - \frac{(m \cdot L_m)^2)}{L_s} \right) \cdot I_{rd} + \frac{m \cdot L_m}{L_s} \cdot \Phi_{sd} \\ \Phi_{rq} = L_r \cdot I_{rq} - \frac{(m \cdot L_m)^2}{L_s} I_{rq} = L_r \cdot \sigma \cdot I_{rq} \end{cases} \quad (16)$$

With :

$$\sigma = 1 - \frac{(m \cdot Lm)^2}{L_s L_r}$$

is the dispersion coefficient of the DFIG. By replacing the expressions of direct and quadrature components of rotor flux (12) in (14), we obtain:

$$\begin{cases} V_{rd} = R_r I_{rd} + Lr \cdot \sigma \cdot \frac{dI_{rd}}{dt} + e_{rd} \\ V_{rq} = R_r I_{rq} + Lr \cdot \sigma \cdot \frac{dI_{rq}}{dt} + e_{rq} + e_\Phi \end{cases} \quad (17)$$

Where:

$$\begin{cases} e_{rd} = -\sigma \cdot L_r \cdot \omega_r \cdot I_{rq} \\ e_{rq} = -\sigma \cdot L_r \cdot \omega_r \cdot I_{rd} \\ e_{\Phi} = \omega_r \cdot \dfrac{m \cdot L_m}{L_s} \cdot \Phi_{sd} \end{cases} \quad (18)$$

The electromagnetic torque Tem can be expressed from the flux and the stator currents by:

$$T_{em} = P \cdot \left(\Phi_{sd} \cdot I_{sq} - \Phi_{sq} \cdot I_{sd}\right) \quad (19)$$

It can also be expressed in terms of the rotor currents and stator flux:

$$T_{em} = P \cdot \frac{m \cdot L_m}{L_s}\left(\Phi_{sq} \cdot I_{rd} - \Phi_{sd} \cdot I_{rq}\right) \quad (20)$$

From (13), the electromagnetic torque becomes:

$$T_{em} = -P \cdot \frac{m \cdot L_m}{L_s} \cdot \Phi_{sd} \cdot I_{rq} \quad (21)$$

The active and reactive stator powers are expressed by:

$$\begin{cases} P_s = -V_{sq} \cdot \dfrac{m \cdot L_m}{L_s} \cdot \Phi_{sd} \cdot I_{rq} \\ Q_s = V_{sq} \cdot \dfrac{V_{sq} \cdot \Phi_{sd}}{L_s} - \dfrac{m \cdot L_m}{L_s} \cdot V_{sq} I_{rd} \end{cases} \quad (22)$$

Expressions (21) and (22) show that The use of dq reference makes the electromagnetic force created by the DFIG, and thus the stator power, proportional to the q-axis rotor current in the scenario where the stator flux sq is held constant (this criterion is fulfilled in the situation of a stable network connected to the stator of the DFIG). Due to the network's constant, reactive stator power is not proportional to d-axis rotor current. As a result, the reactive stator power can be freely adjusted [23].

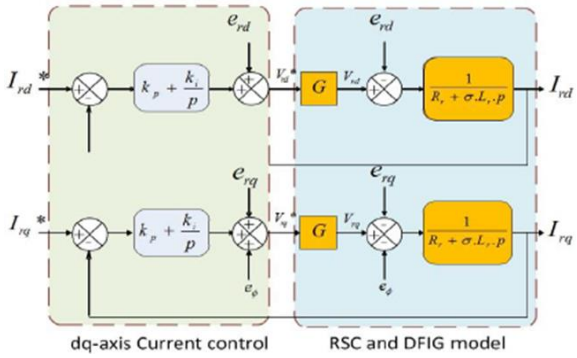

Fig. 6. rotor current regulation on the dq-axis

Assuming that the effect of couplings can be managed of each current separately, the DFIG model in dq reference connected to stator rotating field demonstrates that we may create a rotor currents control. The q-axis rotor current and the d-axis rotor current will be used as reference values for these regulators. To build rotor current control loops, we suppose that the RSC (rotor side converter) is optimal (which correlates to disregarding the wasted time enforced by the power switch drivers) and that the DC/AC converter (RSC) could be described by a gain G which equation is:

$$G = \frac{V_{dc}}{2 \cdot V_p} \quad (23)$$

with: Vp: the magnitude of the triangular carrier of the generation of the PWM. Vdc : voltage of the DC link capacitor. We also suppose that the rotor voltages are the same as their references. Vrk* (k Є [2, 5-12, 15, 20, 22-27]), which means that the magnitude Vp of the carrier should be secured to Vdc / 2, implying a gain G = 1.

The block control loops of the dq axes rotor currents diagram is shown in Fig. 6. The controllers used are PI correctors. The reference of the q-axis rotor current is formed from the MPPT control via reference of electromagnetic torque (21 and 12).

The regulation of the stator reactive power provides the reference current for the d-axis rotor current. The RSC's control block diagram is shown in Figure 7. This method can individually control the dq axis rotor currents, as well as the stator's active and reactive power.

The stator flux must be estimated along the d-axis in order to create the rotor's reference current. The grid is assumed to be stable in our study, and the dq reference choice is connected to the rotational field of the stator. Thus, measurements of the d-axis stator and rotor currents in open loop can be used to determine the d-axis stator flux:

$$\Phi_{sd-est} = L_s I_{sd} + m \cdot L_m \cdot I_{rd} \quad (24)$$

After estimating the stator flux, the dq-axes rotor reference currents must be generated. According to (21), the electromagnetic torque is related to the q-axis rotor current, thus we can construct a relationship between the irq* current and the electromagnetic torque *Tem** from block MPPT control by:

$$I_{rq} *= \frac{L_s}{\text{P.m.L } \Phi_{\text{sd\_est}}} \cdot T_{em} \quad (25)$$

Two approaches for rotor d-axis current reference have been developed in the literature:

- The reactive stator power is controlled by this current.
- The purpose of this current is to reduce Joule losses in the rotor and stator.

Since we have opted to control the value of reactive power in this paper, we will stick with the first method.

$$I_{rd} *= \frac{\Phi_{sd-est}}{m \cdot L_m} - \frac{L_s}{m \cdot L_m \cdot V_{sq}} \cdot Q_s * \quad (26)$$

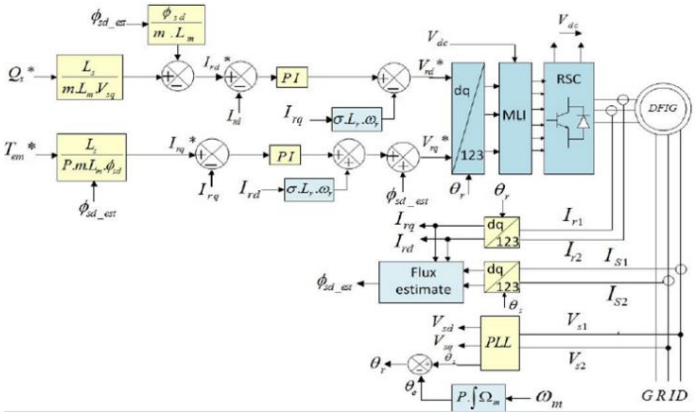

Fig. 7. The Rotor Side Converter's Control Approach (RSC)

Control of the AC/DC converter:

The GSC is an AC/DC converter with an RL filter that connects the DC bus to the electrical network. This converter performs two functions:

- Maintain a steady DC bus voltage independent of the direction and magnitude of the DFIG's rotor power flow.
- Ensure a unity power factor at the point of electrical grid connection.

The instruction of the AC/DC converter is shown in Figure 8. This command carries out the following two tasks:

- Controlling the currents that run through the RL filter
- The DC bus voltage is controlled.

In the dq reference related stator rotating field, (11) becomes:

$$\begin{cases} V_{sd} = V_{gd} - R_g \cdot I_{gd} - L_g \cdot \dfrac{dI_{gd}}{dt} + e_{gd} \\ V_{sq} = V_{sq} - R_g \cdot I_{gq} - L_g \cdot \dfrac{dI_{gq}}{dt} + e_{gq} \end{cases} \quad (27)$$

With

$$\begin{cases} e_{gd=}\omega_s \cdot L_g \cdot I_{gq} \\ e_{gq} = V_{gd} - \omega_s \cdot L_g \cdot I_{gd} \end{cases} \quad (28)$$

Modeling of the AC/DC converter (GSC) connection to the network in the spinning dq stator field reference demonstrates that the current flowing through the RL filter may be changed individually, as can the influence couplings near each axis. These regulators' magnitudes are RL filters in dq axis currents.

In terms of rotor current regulation, the GSC converter model is gain G equal to 1. Figure 9 shows the present technique for block control loops of dq axes. PI controllers are being used. The adjustment terms, dq axis decoupling, and GSC models are shown in these blocks, and they are linked to the network.

The reference dq-axis currents Igd* and Igq* are delivered in the DC bus voltage control and reactive power control blocks at the GSC's grid point of connection, respectively. The below relations describe the active and reactive power exchanged with the electric network:

$$\begin{cases} P_g = V_{gd} \cdot I_{gd} + V_{gq} \cdot I_{gq} \\ Q_g = V_{gq} \cdot I_{gd} - V_{gd} \cdot I_{gq} \end{cases} \quad (29)$$

When losses in the Rg resistance of the RL filter are ignored, and the orientation of the dq reference in relation to the stator rating field (Vgd = 0) is taken into consideration, the (29) become:

$$\begin{cases} P_g = V_{gq} \cdot I_{gq} \\ Q_g = V_{gq} \cdot I_{gd} \end{cases} \quad (30)$$

From (30), imposing the active and reactive power reference, indicated by Pg* and Qg *, imposing reference currents Igd* and Igq*:

$$\begin{cases} I_{gq} *= \dfrac{P_{g*}}{V_{gq}} \\ I_{gd} *= \dfrac{Q_{g*}}{V_{gq}} \end{cases} \quad (31)$$

The reactive power at the GSC's grid connection point is controlled by the direct current element. The DC bus voltage is regulated by the quadrature component. A null reference of reactive power (Qg * = 0 VAr) can be enforced using this technique.

We can write the DC bus powers using (23):

$$\begin{cases} P_{\text{rec}} = V_{dc} \cdot I_{rec} \\ P_c = V_{dc} \cdot I_c \\ P_{\text{ond}} = V_{dc} \cdot I_{\text{ond}} \end{cases} \quad (32)$$

These powers are linked by the relation:

$$P_{rec} = P_c + P_{\text{ond}} \quad (33)$$

IV. Simulation Results and Discussion

The controller design for a DFIG wind turbine has been implemented utilizing Matlab/Simulink to confirm the robustness of the control strategy and then evaluate the performance of the PI controller execution. Tables II and I present the 1 MW doubly-fed induction generator wind turbine parameters. Fig.3 shows the Turbine Power Characteristics at Pitch angle beta = 0 deg. The DFIG wind turbine controller validates the efficiency of a 1MW wind turbine utilizing Matlab software, which had been run with a 400 V RMS voltage at 50Hz per unit system for the simulation, as shown in Fig.4. At the same time, the Simulink model of the wind turbine is shown in Fig.5. The Controller Rotor Side Converter (RSC) and Grid Side Converter (GSC) are shown in Fig.6. In this situation, wind velocity changes whenever a step-change occurs between 8/s and 12 m/s, as seen in Fig 7. The research proposes a state feedback controller for an accurate DFIG wind generation unit model to improve the machine's grid transient response. The wind turbine system's state variable results are depicted in Fig. 8-Fig. 15. Figs. 8 and 9 show the real and reactive power responses of the DFIG wind generation system. Fig. 10 shows the DC link voltage has been improved for the system.

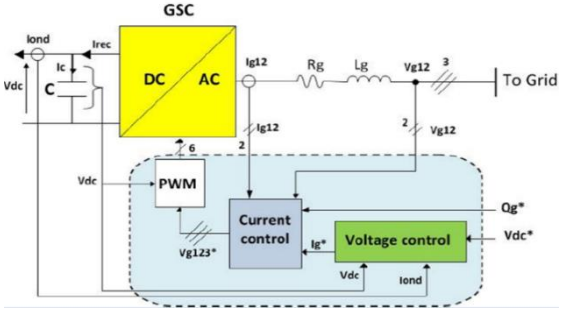

Fig. 8. The Grid Side Converter's command technique (GSC)

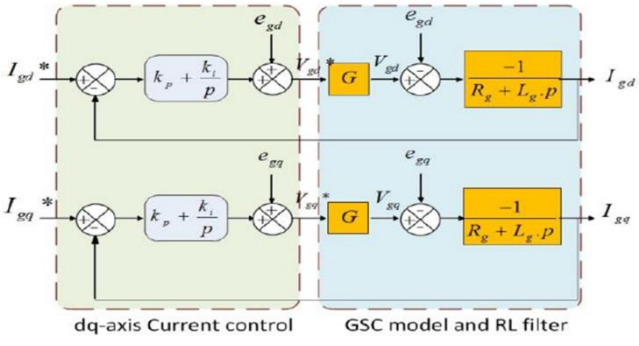

Fig. 9. dq-axis RL filter current control

TABLE I. DFIG PARAMETERS

Parameters	Value	Units
Nominal power	1	MW
Voltage	400	V
Stator resistance	0.00706	PU
Rotor resistance	0.005	PU
Stator self-inductance	0.171	PU
Rotor self-inductance	0.156	PU
Mutual inductance	2.90	PU
Total inertia	5.04	Kg.m^2
Friction Coefficient	0.01	N.mS^{-1}

TABLE II. TURBINE PARAMETERS

Parameters	Value	Unit
Power at point C	0.73	PU/mechanical power
Wind speed at point C	12	m/s

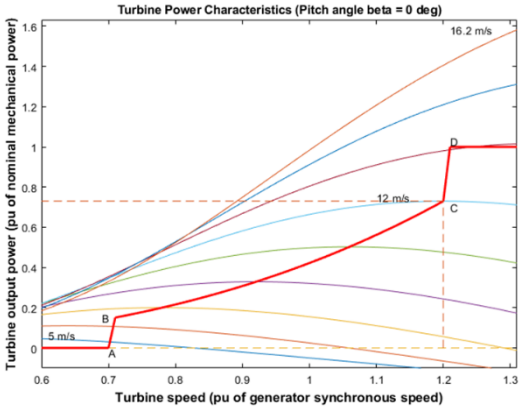

Fig. 10. shows the Turbine Power Characteristics at Pitch angle = 0˚.

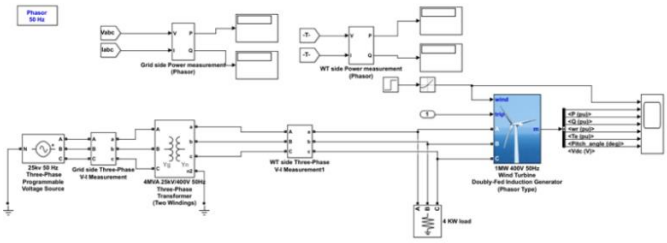

Fig. 11. Simulink model of DFIG wind turbine-load system

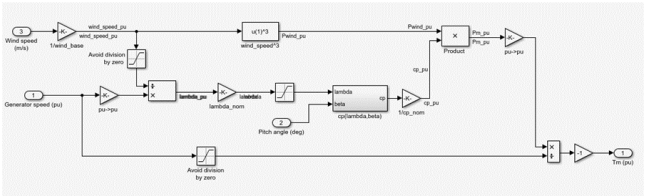

Fig. 12. Simulink model of wind turbine

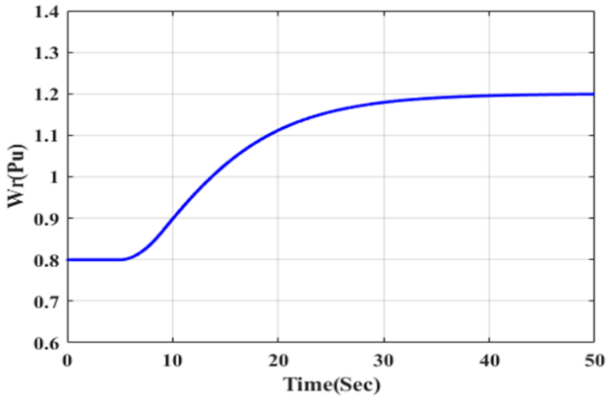

Fig. 13. the Controller Rotor Side Converter (RSC) and Grid Side Converter (GSC)

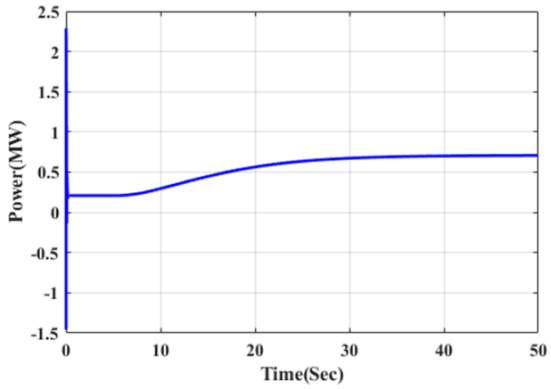

Fig. 14. Step change in Wind speed

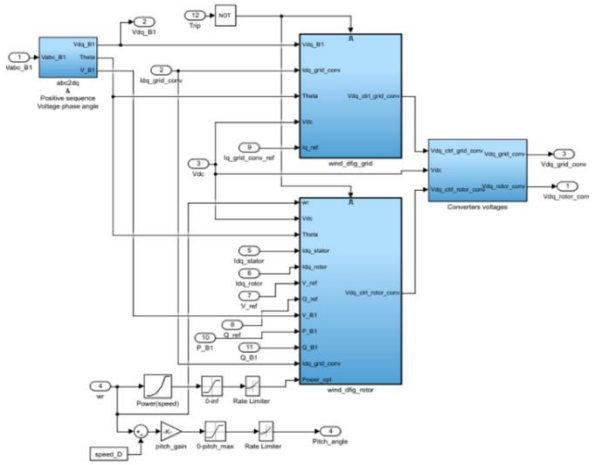

Fig. 15. The real power response of the DFIG wind generation system

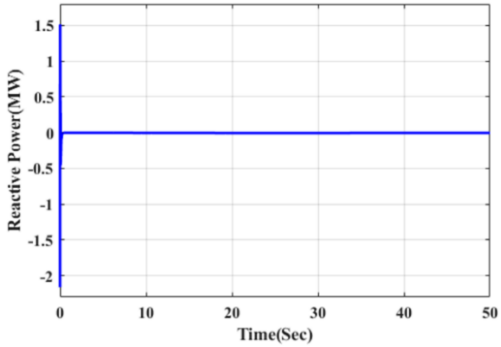

Fig. 16. The reactive power response of the DFIG wind generation system

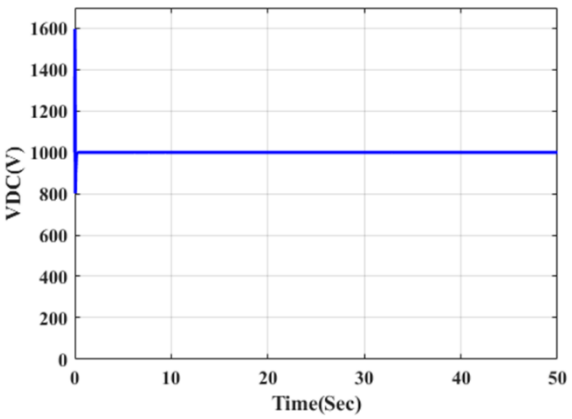

Fig. 17. the DC link voltage

CONCLUSION

The feedback Linearization control approach with a DFIG is developed for the active and reactive power of the wind turbine. It has the potential to increase the wind turbine system's performance dramatically. The DFIG wind turbine was simulated using a wind turbine dynamic model. The results show that sag and overshot of the wind farm's real power and voltage can significantly decrease after the disturbance is eradicated. The damping properties and system stability are improved via feedback approaches. Furthermore, results have been reported on the dynamic response of the system modeling and simulation. It is essential to investigate the analytical features of stability so that the feedback technique used to control the power system can be more successful. Furthermore, the nonlinear dynamic model could be used to create a simple control scheme for the DFIG wind turbine system in the presence of grid voltage disturbances. Finally, to illustrate the feedback technique applications to such a complicated control system, it will be fascinating to analyze the somewhat scenario of a huge energy system analytically.

CONTRUBITION OF THE AUTHORS

The contributions of the authors to the article are equal.

CONFLICT OF INTEREST

There is no conflict of interest between the authors.

STATEMENT OF RESEARCH AND PUBLICATION ETHICS

Research and publication ethics were observed in this study

REFERENCES

[1] H. Abouobaida, "Modeling and Control of Doubly Fed Induction (DFIG) Wind energy conversion system," Journal of Electrical Engineering, vol. 15, no. 1, pp. 12-12, 2015.

[2] S. Ahyaten and J. E. Bahaoui, "Modeling of Wind Turbines Based on DFIG Generator," in Multidisciplinary Digital Publishing Institute Proceedings, 2020, vol. 63, no. 1, p. 16.

[3] D. Chatterjee and Z. H. Rather, "Modelling and Control of DFIG-based Variable Speed Wind Turbine," ed: Indian Academy of Sciences, Bengaluru, India, 2018.

[4] A. Chandana, C. Mutta, and G. V. M. Kiran, "MODELLING AND CONTROLLING OF DFIG BASED WIND SYSTEM USING POWER MATRIX TECHNIQUE," 2018.

[5] Z. Mi, L. Liu, H. Yuan, P. Du, and Y. Wan, "A novel control strategy of DFIG based on the optimization of transfer trajectory at operation points in the islanded power system," Mathematical Problems in Engineering, vol. 2016, 2016.

[6] K. Noussi, A. Abouloifa, H. Katir, and I. Lachkar, "Modeling and control of a wind turbine based on a doubly fed induction generator," in 2019 4th World Conference on Complex Systems (WCCS), 2019: IEEE, pp. 1-5.

[7] B. Qinyu, Y. Lin, M. Jiayi, L. Tianqi, Z. Xiaotian, and W. Youyin, "Study of Double Fed Wind Turbine Modified Simulation Model in Grid Operation," in 2018 China International Conference on Electricity Distribution (CICED), 2018: IEEE, pp. 2023-2028.

[8] R. Rajasekaran and M. Mekala, "Research Issues in DFIG Based Wind Energy System," ELECTRONICS, vol. 22, no. 1, pp. 40-47, 2022.

[9] M. Abulizi, L. Xie, and K. Wang, "Simulation Study of DFIG Wind Turbine under Grid Fault Open-Circuit," in 2019 IEEE 3rd International Conference on Green Energy and Applications (ICGEA), 2019: IEEE, pp. 89-94.

[10] G. S. Kaloi, J. Wang, and M. H. Baloch, "Dynamic modeling and control of DFIG for wind energy conversion system using feedback linearization," Journal of Electrical Engineering and Technology, vol. 11, no. 5, pp. 1137-1146, 2016.

[11] A. G. Abo-Khalil, A. Alghamdi, I. Tlili, and A. M. Eltamaly, "Current controller design for DFIG-based wind turbines using state feedback control," IET Renewable Power Generation, vol. 13, no. 11, pp. 1938-1948, 2019.

[12] A. B. Lajimi, S. A. Gholamian, and M. Shahabi, "Modeling and control of a DFIG-based wind turbine during a grid voltage drop," Engineering, Technology & Applied Science Research, vol. 1, no. 5, pp. 121-125, 2011.

[13] B. Qin, H. Li, X. Zhou, J. Li, and W. Liu, "Low-voltage ride-through techniques in DFIG-based wind turbines: A review," Applied Sciences, vol. 10, no. 6, p. 2154, 2020.

[14] T. M. Masaud and P. Sen, "Modeling and control of doubly fed induction generator for wind power," in 2011 North American Power Symposium, 2011: IEEE, pp. 1-8.

[15] B. Pokharel, Modeling, control and analysis of a doubly fed induction generator based wind turbine system with voltage regulation. Tennessee Technological University, 2011.

[16] D. Li, M. Cai, W. Yang, and J. Wang, "Study of Doubly Fed Induction Generator Wind Turbines for Primary Frequency Control," in 2020 IEEE 4th Conference on Energy Internet and Energy System Integration (EI2): IEEE, pp. 2690-2695.

[17] N. Khemiri and A. Khedher, "A comparison of conventional and modified vector control strategies for controlling transient currents and voltage dips in grid‐connected wind and photovoltaic hybrid system," Environmental Progress & Sustainable Energy, vol. 39, no. 5, p. e13415, 2020.

[18] J. Hu, Y. He, L. Xu, and B. W. Williams, "Improved control of DFIG systems during network unbalance using PI–R current regulators," IEEE Transactions on Industrial Electronics, vol. 56, no. 2, pp. 439-451, 2008.

[19] J. Hu, Y. Huang, D. Wang, H. Yuan, and X. Yuan, "Modeling of grid-connected DFIG-based wind turbines for DC-link voltage stability analysis," IEEE Transactions on Sustainable Energy, vol. 6, no. 4, pp. 1325-1336, 2015.

[20] Z. Dekali, L. Baghli, A. Boumediene, and M. Djemai, "Control of a grid connected DFIG based wind turbine emulator," in 2018 5th International Symposium on Environment-Friendly Energies and Applications (EFEA), 2018: IEEE, pp. 1-6.

[21] G. Abad, J. Lopez, M. Rodriguez, L. Marroyo, and G. Iwanski, Doubly fed induction machine: modeling and control for wind energy generation. John Wiley & Sons, 2011.

[22] M. Nadour, A. Essadki, and T. Nasser, "Coordinated control using backstepping of DFIG-based wind turbine for frequency regulation in high wind energy penetrated system," Mathematical Problems in Engineering, vol. 2020, 2020.

[23] S. Gupta and A. Shukla, "Improved dynamic modelling of DFIG driven wind turbine with algorithm for optimal sharing of reactive power between converters," Sustainable Energy Technologies and Assessments, vol. 51, p. 101961, 2022..

Optimal Power Flow by using Distributed Generation in Six Buses Iraqi Network

Received: 29 July 2022; Revised: 22 August 2022;
Accepted: 25 December 2022
Research Article

Husham Sulaiman Sajir
General Company for Electricity Distrbution Middle
Anbar , Iraq
husham_sl@yahoo.com
ORCID: 0000-0002-6370-2347

Abstract-The OPF problem is discussed in detail in the literature. It is also explained how various methods and techniques can be used to solve it. Finally, a detailed illustration of the LP optimization tool is provided. The complexity of the OPF problem is immense. It involves the various design, planning, and operation problems related to power systems. This report aims to provide an overview of the LP optimization method and its various applications. FOR full AC Increment method. Furthermore, a conceptual review of reactive power pricing was presented, as well as a suggested approach for incorporating the cost function into the goal function. Finally, a quick representation of the toolbox PSAT Simulator was presented, as well as the implementation of both methods on the 6-bus test system using a systematic process, and a comparison of both approaches during the OPF, as well as before and after the inclusion of cost function.

Keywords—OPF, optimal power flow, psat, power system analysis toolbox, LP, liner programming

I. INTRODUCTION

Before the introduction of the optimum approach to share the real load among several thermal productions with an overall capacity higher than the required generation was determined using the optimal power flow, economic dispatch (ED). The best or optimum way to schedule these units to achieve the lowest generating cost while adhering to the entire generation must meet total demand plus losses, according to the restriction. Line overloading was a serious[1] concern and a threat to the economically dispatched power systems until the early 1960s when the network's capacity was nearing its maximum. To protect the system's security, further limits were implemented, and optimal power flow (OPF) was proposed[2]. "The determination of the whole state of the power system with an optimal operation within security limitations" is how an optimal power flow is defined. These restrictions could be described as active and reactive power generation boundaries, bus voltage limits, transformer tab rates, phase shift limits, transmission line thresholds, and possibly the ideal fuel cost and safety for running at that optimal point without breaching any restraints. The various constraints that are associated with the operation of power systems can be represented as different types of limits[3]. These limits can be used to determine the optimal point at which to operate safely and cost-effectively[4]. The problem grew in size and complexity as a result of these constraints[3]. This is solved, however, by combining a mathematical technique for optimization with a power flow calculation. Optimization is described as "the process of minimizing or maximizing an objective function," and it is accomplished using a mathematical optimization tool such as linear optimization, non-linear optimization, and a variety of other methods. The linear programming (LP) method is used to achieve linear optimization. Because of its ability to solve both linear and non-linear objective functions via linearization, as well as its simplicity of managing inequality constraints, LP is one of the most powerful optimization methods. [5].

II. THE POWER FLOW PROBLEM

The goal of the power flow problem is to identify unknown parameters in the network elements of a power system that is expected to be balanced and illustrated by a single line diagram. Hundreds of buses and branches make up the power system network, with impedances stated per unit on a common MVA basis[6]. In terms of node (bus) currents, the nodal admittance form of the network equations yields a complex linear simultaneous equation, resulting in non-linear equations that must be resolved utilizing iterative procedures. The power flow problem is solved using iterative approaches[7]:

- The Gauss Seidel formula.
- The Newton Raphson formula.
- Decoupled power flow solution.

For power system analysis and design, as well as planning and operation, power flow studies are essential. These studies include optimization, sensitivity analysis, economic analysis, voltage stability, transient stability, and contingency analysis. As previously stated, the unknown parameters in the power flow problem must be defined, and the types of buses in the network are used to classify these parameters. [8]. Each bus is related to four quantities:

- The magnitude of the bus voltage |V|.
- The phase angle of the voltage δ.
- The real power of the generator P.
- The reactive power of the generator Q.
- The buses types are classified into:

The Slack bus: also known as the swing bus, serves as a reference bus for calculating the variances in generated power and loads induced by network losses. The voltage magnitude and phase angle are given in this bus, as well as the real and reactive power to be calculated.

Load buses, also known as P-Q buses, are used to determine the real and reactive powers, as well as the voltage magnitude and phase angle.

Regulated buses: also known as P-V buses or voltage-controlled buses, these buses are generator buses with real power and voltage magnitude specifications, as well as the generator reactive power restrictions. The actual power and phase angle to be used are also specified.

III. ECONOMIC DISPATCH

Best possible dispatch, also known as Economic dispatch, is a method of calculating generating unit scheduling in order to lower total operating costs while remaining within the constraints[9]. Total production must equal total demand plus losses[10]. The input-output (I/O) generation cost function causes the ED issue's nonlinearity, while the equalization requirement is the power balancing restriction and the inequality limitation is the generating capacity limits constraint.

Since the idea of scheduling generators to reduce total running costs became popular in the 1920s or perhaps earlier, the economic dispatch problem has existed[11]. Various methods were employed in 1930 to determine the most cost-effective network form: "the base load method" and "the best method." Optimal dispatch, also known as Economic dispatch, is a method of selecting generating unit scheduling to lower overall operating costs while adhering to the constraint that total generation must equal total demand + losses[12]. The input-output (I/O) generation cost function causes the ED issue's nonlinearity, while the equality constraint is the power balancing constraint and the inequality constraint is the generating capacity limits constraint[13]. The economic dispatch challenge has existed since the idea of scheduling generators to lower total running costs became popular in the 1920s or possibly earlier. In 1930, "the base load method" and "the best approach" were used to find the most cost-effective network form[14].

IV. OBJECTIVE FUNCTION

Many electric utilities prefer to use single or multiple-segment linear cost functions to depict their generating cost functions. These functions are represented by the curves in Figure 6.1. If we tried to utilize the lambda iteration search method on the single-segment cost function[15], we would always end up with Pmin or Pmax unless l exactly matched the incremental cost, in which case the value of P would be unknown. To address this issue, we have changed the way we dispatch. We begin by running all units at Pmin, then gradually increase the output of the unit with the lowest additional cost. We choose the next lowest incremental cost segment and raise its output if this unit approaches the right-hand end of a segment or achieves Pmax. Eventually, the unit's output will be raised until the total of all unit outputs matches the total load. At this stage, we assign the last unit to be changed to have a partially loaded generation for one segment. It's worth noting that if two units have the same incremental cost, we could just load them evenly, though any generation allocation to such units is arbitrary. To make this method go quickly, we can develop a table that lists the MW contribution of each segment of each unit (the right-hand end MW minus the left-hand end MW). The table is then sorted by incremental cost in increasing order. We don't have to travel back to the top of the table to seek the next segment because we're looking from the top down. This is a very quick mode of economic dispatch. We'll show how piecewise linear cost functions can be employed in a linear model in the next section.

V. CONSTRAINTS

We start with a nonlinear cost function shown in Figure 1. As shown in Figure2, we can represent this nonlinear function using a series of straight-line segments. The three segments for generator i have shown will be represented as $i1$, $i2$, and $i3$. The Pi variable is replaced with three new variables P_{geni1}, P_{geni2} and P_{geni3} . Each segment will have a slope designated S_{i1}, S_{i2}, S_{i3} (where $S_{i1} < S_{i2} < S_{i3}$); then the cost function itself is now represented as the sum of the cost at P_i^{min} plus the sum of the linear cost for each segment which is simply its slope times the P_{ij} variable. Then

$$F_i(P_i) = F_i(P_{imin}) + S_{i1}P_{i1} + S_{i2}P_{i2} + S_{i3}P_{i3} + S_{in}P_{in} \quad \ldots(1)$$

Where:

$$F_i(P_{imin}) = a + bP_{imin} + cP_{imin}^2$$

For the new values of the generation power Pi:

$$0 \leq P_{genik} \leq P_{genik}^{min} \quad \text{for k=1,2,3}$$

$$P_i = P_{imin} + P_{i1} + P_{i2} + P_{i3} + \cdots + P_{in} \quad \ldots\ldots\ldots\ldots (2)$$

$$S_{ik} = \frac{F_i(P_{gen\,ik+1}) - F_i(P_{gen\,ik})}{(P_{gen\,ik+1}) - (P_{gen\,ik})} \quad \ldots\ldots\ldots\ldots\ldots\ldots\ldots\ldots(3)$$

The cost function is now made up of a linear expression in the three variables P_{geni1}, P_{geni2}, P_{geni3}.

Because the slopes increase in value, the linear program will cause P_{genik} to be at its limit max

$P_{gen\,ik}^{max}$ before $P_{geni(k+1)}$ increases beyond 0.

VI. OVERVIEW OF PSAT

PSAT is a MATLAB toolkit for analyzing and controlling electric power systems. Power Flow, Continued Power Flow, Optimal Power Flow, Small Signal Stability Analysis, and Time Domain Simulation are all included in PSAT[16]. Graphical user interfaces (GUIs) may be used to evaluate all PSAT operations, and a Simulink-based library provides a user-friendly tool for network construction. The power flow routine, which also handles state variable initialization, lies at the heart of PSAT. Further static and/or dynamic analysis can be undertaken once the power flow has been solved. These are the routines:

1. optimal Power flow (OPF)
2. Power flow continuation (CPF)
3. Analysis of small-signal stability
4. Simulations in the time domain
5. Positioning of the phasor measuring unit (PMU).

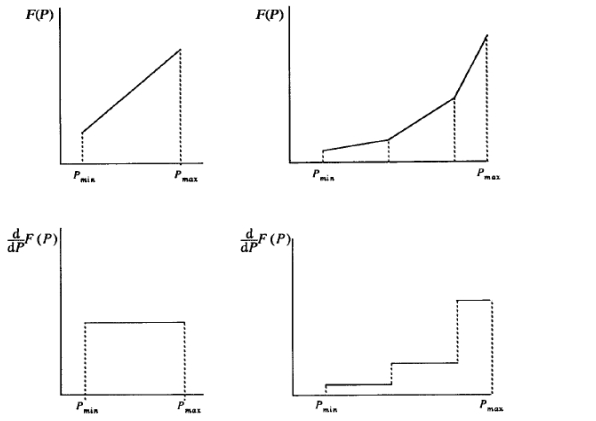

Fig. 1. Piecewise linear cost functions.

VII. THE 6-BUS SYSTEM DESCRIPTION:

The system has six buses, three producing units, and eleven transmission lines. Bus 1 is the slack (reference bus), buses 2 and 3 are P-V buses, and buses 4, 5, and 6 are load (P-Q) buses. The impedances are measured in per-units on a 100 MVA basis[17], with bus voltage restrictions ranging from 1.07pu to 0.95pu. The input data for the power flow and the generating cost functions are also provided[18].

$$F_1(P_1) = 213.1 + 11.669P_1 + 0.00533P_1^2$$

$$F_2(P_2) = 200 + 10.333P_2 + 0.00889P_2^2$$

$$F_3(P_3) = 240 + 10.833P_3 + 0.00741P_3^2$$

Unit 1 limits; $50 \le P1 \le 200$ MW,

Unit 2 limits; $37.5 \le P2 \le 150$ MW.

Unit 3 limits; $45 \le P3 \le 180$ MW.

We will be able to calculate the optimal power flow (OPF) utilizing LP with a load of 300 MW. The main distinction is that the solution will differ from that found using the normal method depending on the number of segments employed. For each cost function, we utilize 1, 3, 5, 10, and 50 segments in the following table, and you can see how the solution gets closer to the same answer as the number of segments grows[19].

TABLE I. DCOPF RESULT.

Bus	Pmin (MW)	Pgen (MW)	Pmax (MW)	Pload (MW)	Lambda ($/MWh)
1	50.000	72.643448	200	0	12.4434
2	37.500	118.693991	150	0	12.4434
3	45.000	108.662561	180	0	12.4434
Total generation cost					4145.2 $/h

Note that increasing the number of segments does not necessarily bring the solution closer to the exact solution. When going from two segments to three segments, the solution actually gets slightly worse in terms of total cost. This is simply because the breakpoints with three segments fall further from the true solution than the two-segment case. As the number of segments is increased to five, ten, and even fifty the solution comes very close to the exact solution.

VIII. PSAT SIMULINK LIBRARY EDITOR

The Simulink library is being used to create the system model as well as to change it by altering the components and data. [20].

This model is loaded in PSAT and the power flow analysis has been conducted for getting the results as shown below.

TABLE II. POWER FLOW REPORT.

POWER FLOW REPORT	
NETWORK STATISTICS	
Buses:	6
Lines:	11
Generators:	3
Loads:	3
SOLUTION STATISTICS	
Number of Iterations:	4.00
Maximum P mismatch [p.u.]	0.00
Maximum Q mismatch [p.u.]	0.00
Power rate [MVA]	100.00

TABLE III. POWER FLOW RESULTS

Bus		**Bus1**	**Bus2**	**Bus3**	**Bus4**	**Bus5**	**Bus6**
V	[p.u.]	1.07	1.05	1.05	1.02	1.02	1.02
phase	[rad]	0.03	0	-0.05	-0.06	-0.09	-0.09
P gen	[p.u.]	1.1	1.48	0.5	0	0	0
Q gen	[p.u.]	0.17	-0.2	0.18	0	0	0
P load	[p.u.]	0	0	0	1	1	1
Q load	[p.u.]	0	0	0	0.15	0.15	0.15
P gen	MW	110	148.31	50	0	0	0
Q gen	MVAR	16.74	-20.14	18.38	0	0	0
P load	MW	0	0	0	100	100	100
Q load	MVAR	0	0	0	15	15	15
VR	[p.u.]	0	-0.02	-0.02	-0.04	-0.05	-0.04

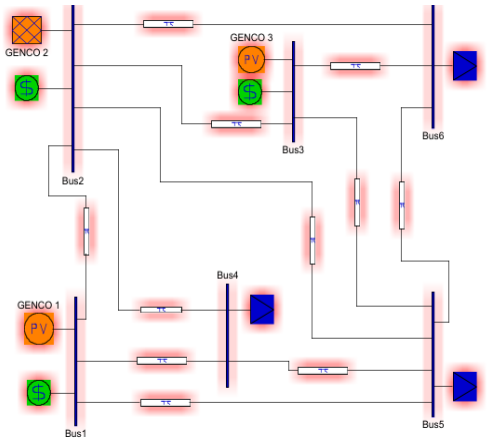

Fig. 2. Simulink 6 bus test system model

TABLE IV. TABLE 4A: LINE FLOWS

From Bus	To Bus	Line	P Flow	Q • Flow	P Loss	Q Loss
			[p.u.]	[p.u.]	[p.u.]	[p.u.]
Bus2	***Bus3***	***1***	0.21	-0.07	0	-0.06
Bus3	***Bus6***	***2***	0.52	0.17	0.01	0.01
Bus4	***Bus5***	***3***	0.07	-0.07	0	-0.08
Bus3	***Bus5***	***4***	0.19	0	0	-0.05
Bus5	***Bus6***	***5***	0.01	-0.04	0	-0.06
Bus2	***Bus4***	***6***	0.61	-0.03	0.02	0.01
Bus1	***Bus2***	***7***	0.16	0.01	0	-0.04
Bus1	***Bus4***	***8***	0.49	0.12	0.01	0
Bus1	***Bus5***	***9***	0.45	0.04	0.01	-0.01
Bus2	***Bus6***	***10***	0.5	-0.04	0.02	-0.01
Bus2	***Bus5***	***11***	0.33	-0.02	0.01	-0.01

TABLE V. TABLE 4B: LINE FLOWS

From Bus	To Bus	Line	P Flow	Q Flow	P Loss	Q Loss
			[p.u.]	**[p.u.]**	**[p.u.]**	**[p.u.]**
Bus3	*Bus2*	*1*	-0.21	0.01	0.00	-0.06
Bus6	*Bus3*	*2*	-0.51	-0.16	0.01	0.01
Bus5	*Bus4*	*3*	-0.07	-0.01	0.00	-0.08
Bus5	*Bus3*	*4*	-0.18	-0.05	0.00	-0.05
Bus6	*Bus5*	*5*	-0.01	-0.02	0.00	-0.06
Bus4	*Bus2*	*6*	-0.59	0.04	0.02	0.01
Bus2	*Bus1*	*7*	-0.16	-0.05	0.00	-0.04
Bus4	Bus1	8	-0.48	-0.12	0.01	0.00
Bus5	Bus1	9	-0.43	-0.05	0.01	-0.01
Bus6	Bus2	10	-0.48	0.03	0.02	-0.01
Bus5	Bus2	11	-0.32	0.00	0.01	-0.01

TABLE VI. POWER EFFICIENCY P.U

P Flow in	P Flow out	efficiency
[p.u.]	*[p.u.]*	*%*
0.21	0.21	99.03%
0.52	0.51	98.95%
0.07	0.07	98.38%
0.19	0.18	97.90%
0.01	0.01	99.79%
0.61	0.59	97.24%
0.16	0.16	98.55%
0.49	0.48	97.67%
0.45	0.43	96.78%
0.50	0.48	96.84%
0.33	0.32	97.04%

IX. RESULTS AND DISCUSSION

The proposed method's performance is tested using a six-bus distribution system. Figure 1 depicts the structure of the 6bus network. The 6bus distribution system has only one generator. Three transformers and one shunt reactive power compensator are located at the slack bus in the system. The overall reactive power load was 45 Mvar, while the total real power load was 300 MW. After one hundred iterations, most of the time there would be no discernible improvement in the optimization outcome. However, to give the particles enough time to approach the global minimum, the optimization process' ending condition is set at two hundred iterations. The swarm has fifty members. In Figure 2, V is the voltage value at the slack bus or PV bus, and T is the transmission line for the range system. At the buses (1,2,3) are power injection. The buses (4,5,6) represent load. The PSAT modeling calculates all energy flow from the slack bus to the load bus. Also using a range system make the load flow more reliable and flexible at the same time to transfer the load.

CONCLUSION

In this paper, power flow simulations of six buses using PSAT are used. An analysis was conducted to calculate the optimal flow of energy and to calculate the transmission losses with the energy consumed by the load compared with the available generation. On the other hand, calculating the capacity spent with losses to provide generation gives the actual need for the system.

The system's transient behavior is determined by the placement of the energy sources and their connection to the best bus for minimizing losses.

This study demonstrates how voltage stability and optimal power flow studies can be carried out simultaneously. Furthermore, applying constraints to the current operating point reduces the space of feasible solutions, resulting in distinct optimal solutions in the maximum distance to collapse problem. It is proven the differences between saddle-node and limit-induced bifurcation. An optimized power flow method with voltage stability criteria is employed on a test system.

CONTRUBITION OF THE AUTHORS

The contributions of the authors to the article are equal.

CONFLICT OF INTEREST

There is no conflict of interest between the authors.

STATEMENT OF RESEARCH AND PUBLICATION ETHICS

Research and publication ethics were observed in this study

REFERENCES

[1] Warid, W., et al., *Optimal power flow using the Jaya algorithm.* Energies, 2016. **9**(9): p. 678.

[2] Anand, R. and V. Balaji, Power flow analysis of simulink IEEE 57 bus test system model using PSAT. Indian Journal of Science and Technology, 2015. 8(23): p. 1.

[3] Cruz, A.A.G. and A.W.R. Canahuire. Small Signal Stability Analysis of Power System of Arequipa using PSAT. in 2020 IEEE XXVII International Conference on Electronics, Electrical Engineering and Computing (INTERCON). 2020. IEEE.

[4] Nitve, B. and R. Naik, Steady state analysis of IEEE-6 Bus System Using PSAT power toolbox. International Journal of Engineering Science and Innovative Technology (IJESIT) Volume, 2014. 3.

[5] Li, S., et al., Optimal power flow by means of improved adaptive differential evolution. Energy, 2020. 198: p. 117314.

[6] Prajapati, C.P. and A.K. Dahiya. Performance improvement of IEEE-30 bus system using UPFC and TCSC on PSAT. in 2019 IEEE Students Conference on Engineering and Systems (SCES). 2019. IEEE.

[7] Stifter, M., et al. Co-simulation of components, controls and power systems based on open-source software. in 2013 IEEE Power & Energy Society General Meeting. 2013. IEEE.

[8] Suganya, R., R. Revathy, and R. Priya. Modeling of Loads Using PSAT in Voltage Stability for Six Bus System. in 2020 International Conference on System, Computation, Automation and Networking (ICSCAN). 2020. IEEE.

[9] Xia, X. and A. Elaiw, Optimal dynamic economic dispatch of generation: A review. Electric power systems research, 2010. 80(8): p. 975-986.

[10] Abbas, G., et al., Solution of an economic dispatch problem through particle swarm optimization: A detailed survey-part I. IEEE Access, 2017. 5: p. 15105-15141.

[11] Elsayed, W.T. and E.F. El-Saadany, A fully decentralized approach for solving the economic dispatch problem. IEEE Transactions on power systems, 2014. 30(4): p. 2179-2189.

[12] Benhamida, F., A dynamic power system economic dispatch enhancement by wind integration considering ramping constraint-application to algerian power system. International Journal of Renewable Energy Research (IJRER), 2015. 5(3): p. 794-805.

[13] Mahmoud, M.S. and M. Fouad, Control and optimization of distributed generation systems. 2015: Springer.

[14] Wang, Z., et al., Chance-constrained economic dispatch with non-Gaussian correlated wind power uncertainty. IEEE Transactions on Power Systems, 2017. 32(6): p. 4880-4893.

[15] Ciornei, I. and E. Kyriakides, A GA-API solution for the economic dispatch of generation in power system operation. IEEE Transactions on power systems, 2011. 27(1): p. 233-242.

[16] Vanfretti, L. and F. Milano, Experience with PSAT (Power System Analysis Toolbox) as free and open-source software for power system education and research. International Journal of Electrical Engineering Education, 2010. 47(1): p. 47-62.

[17] Sarussi, D. and R. Rabinovici. Developing and analysis of power systems using psat software. in 2008 IEEE 25th Convention of Electrical and Electronics Engineers in Israel. 2008. IEEE.

[18] Vijayvargia, A., et al., Comparison between different load flow methodologies by analyzing various bus systems. Int. J. Electr. Eng, 2016. 9(2): p. 127-138.

[19] Peng, Q. and S.H. Low. Distributed algorithm for optimal power flow on a radial network. in 53rd IEEE Conference on decision and control. 2014. IEEE.

[20] Ghosh, S., A. Saha, and N.I. Mou. Load flow simulation of Western grid of bangladesh power system using PSAT and performance-based comparison with PowerWorld. in 2010 International Conference on Intelligent Systems, Modelling and Simulation. 2010. IEEE.

Techno-Economic Analysis of Grid-Connected PV Systems Using BAT Algorithms and Comparison with other Algorithms

Received 5 December 2022; Accepted: 23 December 2022 ***Research Article***

Abdurazaq Elbaz[1]
[1]Libyan Center for Solar Energy Research and Studies
Tripoli, Libya
abdalrazaklabz@gmail.com

***Abstract*— This paper proposed a new approach for optimizing and sizing a grid-connected PV system based on an improved algorithm. The novel and improved bat algorithm (IBAT) for optimization was used, which is principled on teaching processes, with a specific aim of minimizing the total net current cost of these systems. There are several techniques, including the very well-known particle swarm optimization (PSO), in addition to the whale optimization algorithm (WOA), and cuckoo search (CS), that are commonly used to handle this optimization. However, to maximize productivity, novel approaches are required. Optimized grid-connected PV systems, also in countries where fossil fuel is abundant, can reduce production expenses. The grid-connected PV system's net current cost (NPC) and energy cost (COE) are more competitive at $19595 and $0.134/kWh, respectively. The COE and NPC were calculated and then compared with the most used algorithms for optimization, such as PSO, WOA, and CS, with the aim of validating the method proposed herein, and determining the accuracy and speed of the IBAT algorithm. A policy for energy efficiency was then illustrated. The loss of power supply probability (LPSP) was then calculated to determine the degree of operating stability. As the IBAT is both easy to construct and does not require a high number of control parameters, it was determined to be more feasible. The modelled system was tested on a grid-connected PV system installed at the Libyan Center for Solar Energy Research and Studies in Tripoli, Libya. Annual data of irradiance, load profile, and temperature of the PV system were obtained and used for comparing the performances of the IBAT with the other algorithms. Obtained results prove that the proposed IBAT algorithm provides better optimal configuration than commonly used algorithms. The LPSP value of the IBAT algorithm is 0.0965 compared with 0.415, 0.625, and 0.845 for WOA, PSO, and CS, respectively.**

***Keywords*— techno-economic analysis; PV power system; IBAT algorithm; particle swarm optimization; whale optimization; Cuckoo Search.**

I. INTRODUCTION

The growing requirement and necessity of electrical energy added to the cost of oil, and the depletion of fossil fuel sources, combined with environmental pollution as the result of the conventional thermal electric units used to generate energy, have caused great concern worldwide regarding research into alternative methods for electric energy production. To achieve this, grid-connected photovoltaic (GCPV) systems are commonly utilized for injection of the energy that is produced using PV modules in to electrical grids [1] [2].

Currently, the instalment of GCPV systems has become normal practice in a great number of developed countries, including the USA, Spain, and Japan [3]. Aside from the benefits that they provide environmentally, PV systems also offer numerous other benefits, both technically and economically. They are not only beneficial for decreasing losses, but they also offer a significant improvement in the voltage profile of the feeder that they are connected. Moreover, PV system owners are often given incentives by utilities, in the form of a higher sale price for the energy that these systems generate. As an example, Canada's Ontario Power Authority proposed payment of 42 cents/kWh for power that was generated through the use of PV systems as an aspect of their Standard Offer Program, which was established in 2006 [4] [5].

As alternative approaches to traditional methods, techniques of artificial intelligence are becoming more popular. They can learn from examples, overcome nonlinear issues, and very quickly carry out predictions. The most efficient optimization algorithms used in various studies include particle swarm optimization (PSO) [6], genetic algorithms (GAs[7], harmony search algorithms [8] [9], ant colony algorithms[10], simulated annealing[11], cuckoo search (CS) [12], artificial bee colony algorithms[13], hybrid algorithms[14][15], and multi-objective optimization[16]. Different systems and systems of optimization are used in various works, as shown in Table 1. The initial cost of components is very high because of the use of complex structures in these studies. In certain countries, however, the use of grid power is considerably less inexpensive than such complicated systems.

Since solar energy, and in particular PV panels, is among the most utilized renewable systems that can be used in any location, a PV system has been chosen as a power source herein. The suitability of solar radiation in Libya is another reason to use this system. The meteorological data herein comprised real data that was collected from the Libyan Center for Solar Energy Research and Studies in Tripoli, Libya, and hourly loads for the Libyan Center for Solar Energy Research and Studies were also collected as the actual loads that had been registered during the same time. Since real data were the basis of this study, it is possible to use them in an actual a feasibility study implementing the proposed system. In summary, this paper offers contributions to the literature in analysing the performance of a GCPV system based on the concepts of loss of power supply probability (LPSP), net present cost (NPC), and cost of energy (COE), which are indeed significant considerations in such a system.

The optimum system size was determined and performance analysis of a GCPV system was implemented using the improved bat algorithm (IBAT). In solving optimization problems, a comparison of this algorithm with the whale optimization algorithm (WOA), CS, and PSO demonstrates its superiority.

In this study, firstly the mathematical modelling of the grid-connected generation system was explained and the meteorological data for the specific area of study in addition to the load profile were provided. Later, the optimization problem proposed herein was outlined. Finally, the results of the simulation of the newly proposed MATLAB program were discussed.

TABLE I. A SUMMARY OF THE VARIOUS OPTIMIZATION TECHNIQUES THAT WERE USED FOR RENEWABLE ENERGY SYSTEMS IN VARIOUS AREAS.

Reference	Year	Hybrid renewable energy sources	Optimization method	Location
[17]	2018	PV/WT/BAT	GA-PSO and MOPSO	Iran
[18]	2016	PV/WT	HOMER	Saudi Arabia
[19]	2018	PV/WT/FC/BAT	NA	Tunisia
[20]	2011	PV/WT/DG	Direct algorithm	Senegal
[21]	2018	PV/FC	Dispatched control strategy	United Arab Emirates
[22]	2016	PV/WT/FC	Mine blast algorithm	Egypt
[23]	2019	PV/WT/ BT/ DG	Grasshopper optimization alg. (GOA)	Nigeria
[12]	2017	PV/WT	Cuckoo search (CS) algorithm	Algeria
[24]	2016	PV/Combined heat and PowerChip/Battery	Mixed-integer linear	Germany
[25]	2019	PV/WT/Battery	Bat algorithm	Tunisia
[26]	2019	PV/Electrolyzer/ Hydrogen tank/Fuel	Genetic algorithm	Australia
[27]	2017	PV/DG/Battery	Grey wolf optimizer	Algeria
[28]	2019	PV/WT	Crow algorithm	Libya
[29]	2018	PV/WT	RNSYS	Morocco

II. MATHEMATICAL MODEL OF PROPOSED GRID-CONNECTED SYSTEM

The GCPV system that was proposed herein entailed the combination of various components, including a power inverter, solar PV panels (SPVPs), and a utility grid, which are presented in Figure 1.

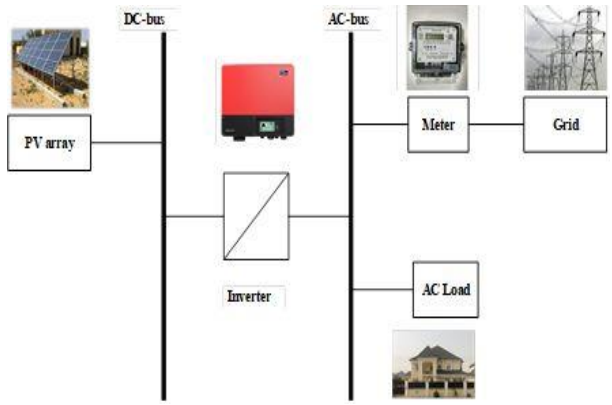

Fig. 1. Diagram illustrating the proposed grid-connected PV system.

III. METEOROLOGICAL DATA OF THE STUDY AREA AND THE LOAD PROFILE

A. Location

The location of this study is the Libyan Center for Solar Energy Research and Studies in Tripoli, located on the Libyan coast of the Mediterranean Sea (32°48.9′N, 13°26.3′E; approximately 6 m above sea level). An application was made for the method proposed herein to be designed and build a GCPV system to contribute power for the Libyan Center for Solar Energy Research and Studies as seen on Figure 2.

B. Solar potential

The air temperature and real solar radiation data of the test location were obtained directly from the climatic database of the Libyan Center for Solar Energy Research and Studies for all of 2019[30].Solar insolation ranged between 1.9 kWh/m^2 and 8.2 kWh/m^2. The minimum temperature recorded was 3 °C and maximum was 45 °C. All data were collected at 5-minute intervals. The 2019 solar radiation profile is presented in Figure 3.

Fig. 2. The designed GCPV system.

Fig. 3. The solar radiation profile for one year.

C. Load profile

For the Libyan Center for Solar Energy Research and Studies in Tripoli, Libya, the actual reported hourly loads over the course of 2019 were collected. As this analysis is focused on real meteorological and load data, it may be beneficial for actual feasibility studies on the introduction of a hybrid green energy system in the region concerned. In Figure 4, the hourly load pattern is provided. With a load averaging 17 kW, the actual load is around 37 kW.

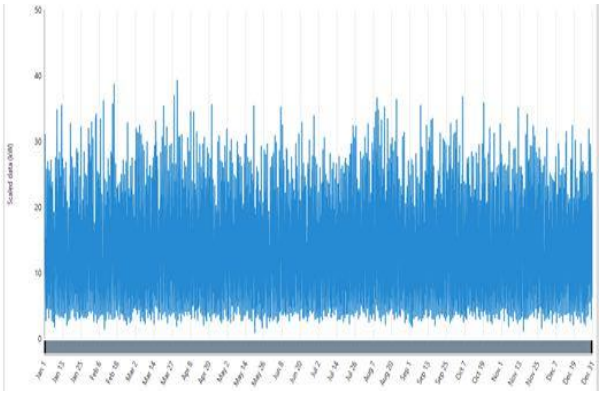

Fig. 4. The load power profile for 2019.

IV. Optimization Problem and Proposed Steps

The proposed system for energy conservation, and steps to be adopted for designing the system in an optimum condition. The proposed GCPV optimization algorithm is summarized in Figure 5. Among the most relevant architectural specifications for GCPV power plants are the seven decision variables shown in green in Figure 5.

A. Total cost of the proposed system

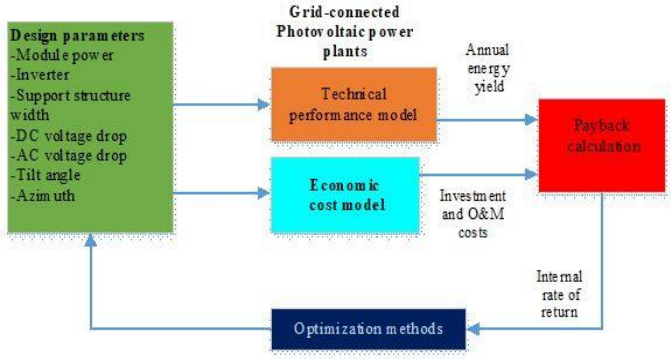

Fig. 5. The design of the optimization process involved in GCPV power plants.

The overall cost for this system is the sum of numerous other costs as calculated investment cost by Equation (1)., where C_{pv} represents the price of a PV panel and N_{pv} project the amount of PV panels used. CRF represents the capital recovery factor, which can be used for converting all these costs to the present value. These can be expressed by Equation (2)., where r represents the interest rate and L_p represents the project lifetime. The start-up investment cost comprises the installation cost for the whole system [31].

The operating cost and maintenance cost of the system are the biggest expenses, and can be calculated by the Equation (3)., where $C_{pvo\&m}$ represents the costs to operate and maintain the presented PV system/unit time and t_{pv} represents the operating time of the PV system. For the yearly cost of operation and maintenance (O&M) of α_{MPV} ($/m^2/year), the sum NPV of the total cost of O&M can be calculated by Equation(4)., where $\mathcal{E}_{PV}$ represents the yearly cost growth rate, A_{PV} represents the PV array total surface area in m^2, and R represents the internal rate of depreciation [32].

$$C_{in} = (C_{Pv}\ N_{PV}) * CRF \quad (1)$$

$$CRF = \frac{r(1+r)^{L_P}}{(1+r)^{L_P}-1} \quad (2)$$

$$C_{o\&m} = C_{pvo\&m} * t_{pv} \quad (3)$$

$$OM_{NPV_{PV}} = \alpha_{OMPV} * A_{PV} * \sum_{K=1}^{N}\left(\frac{1+\mathcal{E}_{PV}}{1+r}\right)^{j} \quad (4)$$

Due to bidirectional flowing of the energy in the system, the cost can be calculated in two different parts. The cost for the power that is procured from the grid C_{gp} and the supplied power to the grid C_{gs} can be calculated by the Equation (5) and Equation(6)., where C_p and C_g represent the cost/unit for the purchased power and the supplied power to the grid, and N_{gp} and N_{gs} represent the cumulative procured and supplied power amounts to the grid, respectively [33].

$$C_{gp} = N_{gp} * C_p \quad (5)$$

$$C_{gs} = N_{gs} * C_s \quad (6)$$

The total costs of system consist of replacement cost C_r, which comprises all replaced parts of system along the running period because of defect or aging, in addition to all the expenses explained above. The replacement cost C_r is important if the lifespan of any of the components is not correlated with project lifetime. So, the total cost of the system can be calculated by the Equation(7) [34].

$$C_{total} = C_{A\ in} + C_{o\&m} + C_{gp} - C_{gs} + C_r \quad (7)$$

B. Constraints and optimized parameters

Net present value (NPV) represents a reliable budgeting method because it makes allowances for the time value of money using discounted cash flows. It entails estimating net cash flows that may be encountered at any time in the future, using a discount rate to discount these flows, and, using the project risk level, then deducting the net start-up investment from the present-day value of these net cash flows, as can be seen in Equation(8), where *IRR* represents the internal rate of return, projected to be 10%; and n represents the predicted running period in years, and C_{ashin} represents the cash inflow, which can be measured as seen on Equation(9) [34].

The payback period comprises the duration of time when the cash outflow of the original start-up investment is considered to have been finally regained the investment. It is an extremely uncomplicated appraisal technique that can be calculated as seen on Equation (10). And Cost of energy (COE) can be calculated by using the Equation(11) [35].

$$NPV = \left(Cash_{in} * \frac{1-(1+IRR)^{-n}}{IRR}\right) - \left(C_{in} + C_{gp}\right) \quad (8)$$

$$Cash_{in} = kWh_{price} * Load \quad (9)$$

$$Payback\ Period = \frac{C_{in}(initial\ investment)}{Cash_{in}} \quad (10)$$

$$COE = \frac{(Total\ cost\ of\ generated\ energy\ for\ one\ year)}{(Total\ energy\ supplied\ in\ one\ year,\ kWh)} \quad (11)$$

In this model, the reliability that this system possesses is tested using the LPSP, which can be explained as a load which the system is incapable of fulfilling in the study period divided by the total load and can be calculated by Equation (12). The value of the LPSP is in the range of [0, 1], which confirms the system's efficiency until the total provided power from the integrated grid-connected solar PV system covers the load. While LPSP values of 0 mean that the load is always fully met, a value of 1 indicates that the required load is totally unmet. Permissible LPSP values are usually believed to be 0.05 or 5%. To minimize the COE with a stable method, the variable to be considered is NPV. The suggested restrictions are seen on Equation(13), where N_{PV} min and N_{PVmax} represent the minimum and maximum amount of PV panels, respectively [24] [35].

V.

$$LPSP = \frac{\sum(P_{load} - P_{PV} - P_{GO})}{P_{load}} \quad (12)$$

$$N_{PVmin} \leq N_{PV} \leq N_{PVmax.} \quad (13)$$

VI. Results And Discussions

The algorithm that was newly proposed herein was applied for investigation of an autonomous electrical grid-connected PV system, used by the Libyan Center for Solar Energy Research and Studies in Tripoli, Libya. The experimental data that were used herein for the solar insolation in 2019 were collected from the Libyan Center for Solar Energy Research and Studies meteorological station. The data were recorded at 5-min intervals and the mean/hour was used for this study. Costs associated with the components of the GCPV system are tabulated in Table 2. The environment provided within MATLAB was used for the implementation and coding of the algorithm that was newly proposed herein, which was conducted on an Intel Core i7-7500U CPU @ 2.9 GHz. A comparison of the performance of this newly proposed method was performed with other metaheuristic approaches, namely the PSO, WOA, and CS algorithms.

The MATLAB Software was used for the implementation and coding of the algorithms to compare the performance of proposed algorithm and the PSO, WOA, and CS, and the results were tabulated. The algorithm parameters are modified to maximize the objective function used in this study as seen below:

- **PSO:** Number of iterations = 100, size of the swarm = 60, C1 = 2, C2 = 2, inertia weight (ω) = 0.7.
- **CS:** Number of iterations = 100, number of nests = 7, alien egg discovery rate = 0.25, Beta (β) = 1.5, Levy multiplying coefficient = 0.1.
- **WOA:** Number of iterations = 100, population (N) = 50, r (random number) in [0,1], a (distance control parameter) decreased from 2 to 0.
- **IBAT:** Population (N) = 50, Number of iterations = 100, Loudness (A) = 0.95, pulse rate (r) = 0.45, Minimum frequency (f_{min}) = 0, parameters to improve the algorithm's performance and regularized the result (w_{Min}, w_{Max}) ∈ [0.5, 1], velocity (V_{max})=10.

We compared the results using most used, well-known, and strong algorithms with the IBAT algorithm to determine validity of the results. The results of IBAT are compared with the outcomes of the WOA, PSO, and CS algorithms.

A particle population travels within the optimization problem's search space in the PSO, WOA, and CS. The particle location constitutes a possible way to solve the optimization problem. Each one of the particles performs a scan of the search space searching for a better location. Herein, one of the terminal criteria is a certain and specific number of iterations. The size of each of the systems is equal to one final total price, and there are two objective functions that minimize the COE and NPC. For all the algorithms, the search space was the same and the variables were the sizes of the components. Table 3 provides a comparison of the algorithm parameters as well as the statistical results of the two specific criteria, as an indicator of the robustness of the algorithms. Determined in this table were the minimum (min), maximum (max), and mean NPC and COE values, respectively. As can be seen, for the three objective functions, the results for the IBAT algorithm were the best with regards to the min, max, and mean values.

The best LPSP is obtained by the proposed IBAT at 0.0965, while the worst is obtained via CS at 0.845. In determining the optimum size of the GCPV system, these observations affirm the superiority of the proposed IBAT algorithm. Figure 6 shows bar charts of the COE and LPSP values that were obtained using the specified approaches. The problem with the PSO, CS, and WOA lies in assigning many PV panels, which leads to secure operation but a solution that is uneconomical. The proposed IBAT algorithm gives a preferable structure for the GCPV system as there is not significant surplus power as seen with the other approaches. This confirms the ability of the proposed GCPV system to achieve secure and economic operation.

TABLE II. COST RELATED TO GCPV SYSTEM COMPONENTS.

	Initial capital costs	Replacement costs	Maintenance costs (/year)	Lifetime (years)
PV array	2800 $/kW	Null	15 $/kW	25
Inverter	327 $/kW	359 $/kW	28 $/kW	10
Structures	$1930	Null	$20	25
Total cost	$17565	$1795	$235	

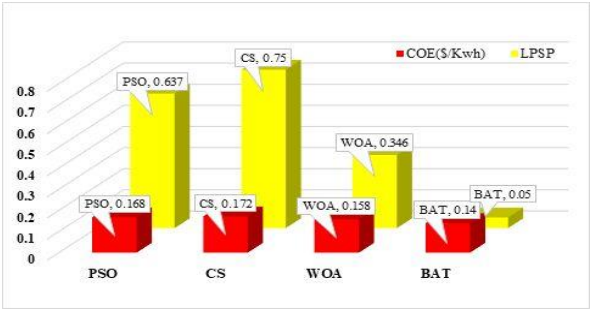

Fig. 6. COE and LPSP values were obtained using the optimization techniques.

TABLE III. TECHNICAL PARAMETERS OF THE CS, PSO, WOA, AND IBAT, AND STATISTICAL RESULTS

Algorithm	NPC ($)			COE ($/kWh)			LPSP
	max	*mean*	*min*	*min*	*mean*	*max*	
IBAT	19760	19604.8	19595	0.134	0.136	0.14	0.0965
WOA	19761	19611	19600	0.151	0.153	0.158	0.415
PSO	19768	19617	19607	0.159	0.161	0.168	0.625
CS	19778	19620	19612	0.165	0.167	0.172	0.845

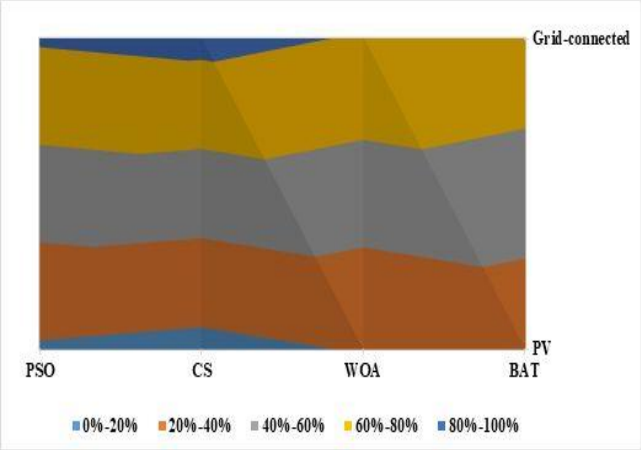

Fig. 7. Annual contributions from PV and grid-connected components using various methods.

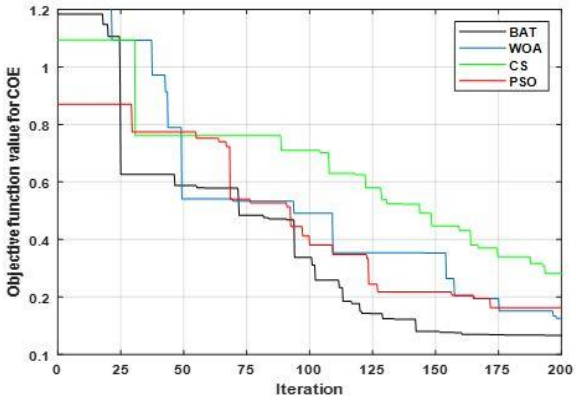

Fig. 8. Comparison between algorithms' convergences for minimum COE ($/kWh).

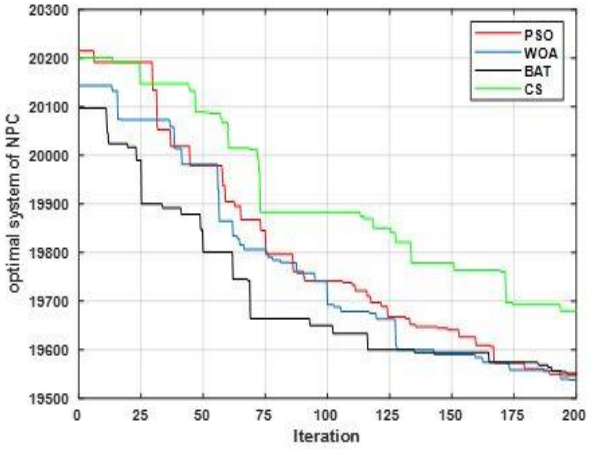

Fig. 9. Comparison between algorithms' convergences for minimum NPC ($).

The percentages of participation for each of the energy sources in attaining the annual load that were obtained using the IBAT proposed herein, and the other algorithms are shown in Figure 7. With this newly proposed methodology that was presented herein, the constricted PV system was able to cover 26% of the load, while 74% of the energy required was grid-connected. Regarding the other optimization methods, the PV system contributes 18%, 15%, and 21%, respectively, via PSO, CS, and WOA, while 82%, 85%, and 79% of the load is grid-connected.

The trends of the NPC and COE in attaining the optimal solution are presented in Figures 8 and 9, where it is seen that the IBAT algorithm achieved the optimal solution more quickly than WOA, PSO, and CS, further demonstrating the convergence speed advantage that the IBAT possesses. With the progression of the algorithm, it was able to find new answers and the NPC and COE values decreased. IBAT's trends are depicted in the figures, depicted via a black line. This algorithm was able to exhibit the most rapid movement to the minimum solution. As was seen using the NPC, the IBAT also exhibited the fastest convergence speed for the COE criterion. In addition to ease of implementation, these benefits result in the IBAT being among the most powerful of the algorithms.

CONCLUSIONS

In this paper, a GCPV system has been presented as a system for power generation to contribute electricity for public places during business hours. Since PV systems that have batteries are more expensive in comparison with PV systems that do not have batteries, the most reasonable use of PV system equipment is in GCPV system installations to contribute to the electricity demand for the daytime period only. In the optimum techno-economic analysis of the proposed method, the IBAT algorithm was used, and the last objective function entailed the minimization of both the NPC and COE.

We compared the IBAT algorithm, and the WOA, PSO, and CS showed the superiority of IBAT for optimization problem solving. In the optimally sized system for the Libyan Center for Solar Energy Research and Studies, the PV panels met an average of 26% of the consumption and the electrical grid was able to supply the remaining electrical load. In contrast, with the other three algorithms, the NPC and COE

had 12.7% and 13.4% increases, respectively. The GCPV system designed here is installed at the Libyan Center for Solar Energy Research and Studies in Tripoli, Libya, and this study used annual real electrical and climatic data recorded by the Libyan Center for Solar Energy Research and Studies. The results obtained with IBAT were compared to WOA, PSO, and CS, and the proposed algorithm exhibited the most superior optimal architecture for the GCPV system, achieving a LPSP of 0.0965 and a COE of 0.1359 $/kWh. The elapsed time of the IBAT approach was 497.326 s, comprising the best time when compared to the other the approaches presented.

CONTRUBITION OF THE AUTHORS

The contributions of the authors to the article are equal.

CONFLICT OF INTEREST

There is no conflict of interest between the authors.

STATEMENT OF RESEARCH AND PUBLICATION ETHICS

Research and publication ethics were observed in this study

REFERENCES

[1] D. J. Swider *et al*., "Conditions and costs for renewables electricity grid connection : Examples in Europe," vol. 33, pp. 1832–1842, 2008, doi: 10.1016/j.renene.2007.11.005.

[2] J. Deb, Y. G. Yohanis, and B. Norton, "The impact of array inclination and orientation on the performance of a grid-connected photovoltaic system," vol. 32, pp. 118–140, 2007, doi: 10.1016/j.renene.2006.05.006.

[3] A. W. Sawab, "Transactions on Energy Conversion," vol. 11, no. 3, pp. 595–600, 1996.

[4] W. A. Omran, M. Kazerani, S. Member, and M. M. A. Salama, "Investigation of Methods for Reduction of Power Fluctuations Generated From Large Grid-Connected Photovoltaic Systems," vol. 26, no. 1, pp. 318–327, 2011.

[5] N. Srisaen and A. Sangswang, "Effects of PV Grid-Connected System Location on a Distribution System," vol. 00, pp. 852–855, 2006.

[6] Y. Sawle, S. C. Gupta, and A. K. Bohre, "Review of hybrid renewable energy systems with comparative analysis of o ff -grid hybrid system Loss of Power Supply Probability Loss of Load Probability," *Renew. Sustain. Energy Rev.*, vol. 81, no. June 2017, pp. 2217–2235, 2018, doi: 10.1016/j.rser.2017.06.033.

[7] J. Khoury, R. Mbayed, G. Salloum, and E. Monmasson, "Optimal sizing of a residential PV-battery backup for an intermittent primary energy source under realistic constraints," *Energy Build.*, vol. 105, pp. 206–216, 2015, doi: 10.1016/j.enbuild.2015.07.045.

[8] M. Paulitschke, "ScienceDirect ScienceDirect Comparison particle swarm and genetic based design The of on District algorithm Heating and Cooling algorithms for PV-hybrid systems with battery and hydrogen storage Assessing the feasibility of path using the heat demand-outd," *Energy Procedia*, vol. 135, pp. 452–463, 2017, doi: 10.1016/j.egypro.2017.09.509.

[9] A. Chauhan and R. P. Saini, "Discrete harmony search based size optimization of Integrated Renewable Energy System for remote rural areas of Uttarakhand state in India," *Renew. Energy*, vol. 94, pp. 587–604, 2016, doi: 10.1016/j.renene.2016.03.079.

[10] C. K. Shiva and V. Mukherjee, "A novel quasi-oppositional harmony search algorithm for automatic generation control of power system," *Appl. Soft Comput. J.*, vol. 35, pp. 749–765, 2015, doi: 10.1016/j.asoc.2015.05.054.

[11] A. Fetanat and E. Khorasaninejad, "Size optimization for hybrid photovoltaic – wind energy system using ant colony optimization for continuous domains based integer programming," *Appl. Soft Comput. J.*, vol. 31, pp. 196–209, 2015, doi: 10.1016/j.asoc.2015.02.047.

[12] O. Nadjemi, T. Nacer, A. Hamidat, and H. Salhi, "Optimal hybrid PV / wind energy system sizing : Application of cuckoo search algorithm for Algerian dairy farms," *Renew. Sustain. Energy Rev.*, vol. 70, no. December 2016, pp. 1352–1365, 2017, doi: 10.1016/j.rser.2016.12.038.

[13] C. K. Das, O. Bass, G. Kothapalli, T. S. Mahmoud, and D. Habibi, "Optimal placement of distributed energy storage systems in distribution networks using artificial bee colony algorithm," *Appl. Energy*, vol. 232, no. July, pp. 212–228, 2018, doi: 10.1016/j.apenergy.2018.07.100.

[14] M. Tahani, N. Babayan, and A. Pouyaei, "Optimization of PV / Wind / Battery stand-alone system , using hybrid FPA / SA algorithm and CFD simulation , case study : Tehran," *Energy Convers. Manag.*, vol. 106, pp. 644–659, 2015, doi: 10.1016/j.enconman.2015.10.011.

[15] M. Lasheen and M. Abdel-salam, "Maximum power point tracking using Hill Climbing and ANFIS techniques for PV applications : A review and a novel hybrid approach," *Energy Convers. Manag.*, vol. 171, no. June, pp. 1002–1019, 2018, doi: 10.1016/j.enconman.2018.06.003.

[16] Z. Huang, Z. Xie, C. Zhang, S. Hwa, and Y. Xie, "Modeling and multi-objective optimization of a stand-alone PV-hydrogen- retired EV battery hybrid energy system," vol. 181, no. August 2018, pp. 80–92, 2019, doi: 10.1016/j.enconman.2018.11.079.

[17] N. Ghorbani, A. Kasaeian, A. Toopshekan, and L. Bahrami, "Optimizing a hybrid wind-PV-battery system using GA-PSO and MOPSO for reducing cost and increasing reliability," *Energy*, vol. 154, pp. 581–591, 2018, doi: 10.1016/j.energy.2017.12.057.

[18] M. A. M. Ramli, A. Hiendro, and Y. A. Al-turki, "Techno-economic energy analysis of wind / solar hybrid system : Case study for western coastal area of Saudi Arabia," *Renew. Energy*, vol. 91, pp. 374–385, 2016, doi: 10.1016/j.renene.2016.01.071.

[19] A. Khiareddine, C. Ben, D. Rekioua, and M. Faouzi, "Sizing methodology for hybrid photovoltaic / wind / hydrogen / battery integrated to energy management strategy for pumping system," *Energy*, vol. 153, pp. 743–762, 2018, doi: 10.1016/j.energy.2018.04.073.

[20] R. Belfkira, L. Zhang, and G. Barakat, "Optimal sizing study of hybrid wind / PV / diesel power generation unit," *Sol. Energy*, vol. 85, no. 1, pp. 100–110, 2011, doi: 10.1016/j.solener.2010.10.018.

[21] C. Ghenai, T. Salameh, and A. Merabet, "ScienceDirect Technico-economic analysis of off grid solar PV / Fuel cell energy system for residential community in desert region," *Int. J. Hydrogen Energy*, vol. 45, no. 20, pp. 11460–11470, 2018, doi: 10.1016/j.ijhydene.2018.05.110.

[22] A. Fathy, "A reliable methodology based on mine blast optimization algorithm for optimal sizing of hybrid PV-wind-FC system for remote area in Egypt," *Renew. Energy*, vol. 95, pp. 367–380, 2016, doi: 10.1016/j.renene.2016.04.030.

[23] A. L. Bukar, C. W. Tan, and K. Y. Lau, "Optimal sizing of an autonomous photovoltaic/wind/battery/diesel generator microgrid using grasshopper optimization algorithm," *Sol. Energy*, vol. 188, no. May, pp. 685–696, 2019, doi: 10.1016/j.solener.2019.06.050.

[24] T. Beck, H. Kondziella, G. Huard, and T. Bruckner, "Assessing the influence of the temporal resolution of electrical load and PV generation profiles on self-consumption and sizing of PV-battery systems," *Appl. Energy*, vol. 173, pp. 331–342, 2016, doi: 10.1016/j.apenergy.2016.04.050.

[25] N. Marsa, L. Houcine, A. Zaafouri, and A. Chaari, "Optimal sizing of stand-alone hybrid photovoltaic / wind system using BAT algorithm," *Int. J. Ambient Energy*, vol. 0, no. 0, pp. 1–9, 2019, doi: 10.1080/01430750.2019.1573756.

[26] J. Assaf and B. Shabani, "A novel hybrid renewable solar energy solution for continuous heat and power supply to standalone-alone applications with ultimate reliability and cost effectiveness," *Renew. Energy*, vol. 138, pp. 509–520, 2019, doi: 10.1016/j.renene.2019.01.099.

[27] A. Yahiaoui, F. Fodhil, K. Benmansour, M. Tadjine, and N. Cheggaga, "Grey wolf optimizer for optimal design of hybrid renewable energy system PV-Diesel Generator-Battery : Application to the case of Djanet city of Algeria," *Sol. Energy*, vol. 158, no. October, pp. 941–951, 2017, doi: 10.1016/j.solener.2017.10.040.

[28] A. Elbaz, A. P. Swarm, and O. Pso, "Using Crow Algorithm for Optimizing Size of Wind Power Plant / Hybrid PV in Libya," no. 1, pp. 19–22, 2019.

[29] A. Laknizi, M. Bouya, A. Astito, and A. Ben, "Sizing a PV-Wind based hybrid system using deterministic approach," *Energy Convers. Manag.*, vol. 169, no. May, pp. 137–148, 2018, doi: 10.1016/j.enconman.2018.05.034.

[30] CSERS, "Centre for Solar Energy Research and Studies." https://csers.ly/en/

[31] L. Xu, X. Ruan, C. Mao, B. Zhang, and Y. Luo, "An improved optimal sizing method for wind-solar-battery hybrid power system," *IEEE Trans. Sustain. Energy*, vol. 4, no. 3, pp. 774–785, 2013, doi: 10.1109/TSTE.2012.2228509.

[32] F. Caballero, E. Sauma, and F. Yanine, "Business optimal design of a grid-connected hybrid PV (photovoltaic) - wind energy system without energy storage for an Easter Island ' s block," *Energy*, vol. 61, pp. 248–261, 2013, doi: 10.1016/j.energy.2013.08.030.

[33] M. Ali, Y. Jahromi, S. Farahat, and S. Masoud, "Civil Engineering and Environmental Systems Optimal size and cost analysis of stand-alone hybrid wind / photovoltaic power-generation systems," vol. 6608, 2014, doi: 10.1080/10286608.2013.853752.

[34] M. Gómez, A. López, and F. Jurado, "Optimal placement and sizing from standpoint of the investor of Photovoltaics Grid-Connected Systems using Binary Particle Swarm Optimization," *Appl. Energy*, vol. 87, no. 6, pp. 1911–1918, 2010, doi: 10.1016/j.apenergy.2009.12.021.

[35] E. Drury, P. Denholm, R. Margolis, E. Drury, P. Denholm, and R. Margolis, "The Impact of Different Economic Performance Metrics on the Perceived Value of Solar Photovoltaics The Impact of Different Economic Performance Metrics on the Perceived Value of Solar Photovoltaics," no. October, 2011.

[36]

Performance Analysis Rectangular Patch Antenna 3.5 GHz for Wi-Max and WLAN

Received 12 December 2022; Accepted: 22 December 2022 *Reseaech Article*

Ali Abozied
aliradar@yahoo.com
0000-0001-9318-941X

Abdelaziz Al Dawi
azizedowi@gmail.com
0000-0003-1356-7914

Cihat Seker
Electrical and Electronic Engineering
Karabuk University
Karabuk ,Turkey
cihatseker@karabuk.edu.tr

Abstract—This paper gives the layout and evaluation of a brand-new shape of -hollow rectangular microstrip patch antennas for wi-fi telecommunication programs below the sub-5GHz recurrence band. The prepared patch antenna is appropriate for WiMAX programs worked at 3.5GHz aimed to offer elevation velocity statistics charges and net get admission to for a huge insurance range. The rectangular patch layout supplied on this study exhibited higher overall performance in phrases of put down in area, development in voltage status wave ratio much less than 1.2, impedance and overall performance, is advanced via way of means of putting square slots Simulation end result received the use of CST 2021 software. The patch antenna turned into prepared a FR4 lossy substrate with dielectric permittivity of 4.3 and 1.55mm wideness the use of an ordinary feed line. The patch layout supplied on this study exhibited higher overall performance in phrases of minimization in region, development in benefit and straight with appreciate to the rectangular antenna layout. The cost of every belonging is numerous in order that the overall performance of the antenna along with go back loss, benefit, straight, beam sample and bandwidth at 3.5 GHz may be analyzed. For destiny work, the simulations must be done at tinier period length and wide field. Besides that, the wideness of the substrate may be numerous and the overall performance may be analyzed.

Keywords—patch antenna, WiMAX, VSWR, gain, performance

I. INTRODUCTION

Antennas are developing rapidly due to the interest of researchers due to their need for different uses, mostly in wi-fi verbal exchange software as it gives numerous benefits including little size, easy structure, smooth fabrication, and occasional cost. furthermore, a microstrip antenna has positive barriers including low benefit, little efficiency, slim, impedance and bandwidth. therefore, the scientific research purpose is to enhance the benefit. One of the rapidly growing wi-fi verbal exchange structures is the Wi-Max because of its extensive insurance part. Invest with the IEEE 802.sixteen standard, 3.5 GHz are allotted frequencies for WiMAX applications. that's appropriate for Industrial Scientific and Medical. therefore, the dual-band and multi-band resonant conduct of published and slot antennas may be produced with the aid of using making use of fractal geometries to regulate the antenna slot structures Alone the difficult problems in microwave engineering is to layout compact, high-performance, and wideband antennas. Among the strategies which might be carried out for antenna compactness, miniaturization, and bandwidth enhancement in shifting in the direction of to 5G systems, many research had been performed on patch antennas due to their compactness, reasonably-priced and speedy manufacturing. In this studies paper, a rectangular antenna is proposed for dual-band operation focused at 3.5 GHz for Wi-Max software. It carries slots withinside the patch to achieve appropriate benefit, VSWR, impedance and bandwidth on the preferred frequencies.

Therefore, improvement of wi-fi networks is critical due to the fact 5G generation makes use of rising frequency bands and huge sign bandwidth to growth the transmission bit charge, for this reason supplying higher insurance with much less strength consumption. Be advanced withinside the wi-fi 4G and 5G communique technology to fulfill the desired overall performance. wireless communication is a couple of structures convergence in cellular data get entry to technologies. Consequently 3.5 GHz has large utility potentialities in 5G implementation. In a cellular data communications system, one of fundamental desires is to recognition on subsequent technology via a few required have to acquire are better statistics charge utility and offerings which includes a picture withinside the nearby insurance network, net browsing, cellular data teleconference and multimedia. This predominant task element for subsequent generations. For maximum cell statistics wherein inner visitors is generated, antenna distribution performs a more and more substantial function in indoor wi-fi communique structures. In addition, to offer higher communique offerings, many frequency bands are designed and commercially utilized in one-of-a-kind communications structures which includes 4G WiMAX and cellular data nearby vicinity network WLAN. Therefore, a successful broadband distribution antenna is needed in concurrently assembly a couple of provider frequency bands. The antenna with many advantages, which includes little size, lowest price, and smooth integration with lively circuits; appropriate for multi-band layout and dual-polarization antennas, are extensively utilized in revealed circuits. Main downside of microstrip patch antenna is its slender bandwidth. Therefore, many strategies were used to growth the bandwidth finally, in this paper, an antenna running at 3.5GHz can be designed the usage of CST software. This recurrence is chosen as used the 5G running frequency, and their overall performance can be analyzed

The goal is to own a high advantage and performance to make sure that the foremost records switches in any wi-fi communication space antenna are the amount one requirement. once birth out any microstrip patch antenna, several improvement ways are used, and twin feed. Wide information measure antennas are applied for a huge type of

community frequencies, that are larger inexperienced for a few distance space implementations. With a twin-feed antenna, section distinction is simple to maintain the foremost common issue in wi-fi communication is the orientation of receivers and transmitters. Multiband operation and antenna length miniaturization could also be performed by utilizing the noted options of self-similarity and area filling.

II. PROPOSED RECTANGULAR ANTENNA.

The important three layout parameters of antenna are the ringing recurrence (fr), relative permittivity of the substrate (εr) and the density of the substrate (h). The ringing recurrence of the antenna needs to be appropriate for the WiMAX, 3.5 GHz. The patch is product of FR4 lossy substrate layers which have a permittivity (Ɛr) of 4.30, a loss tangent (tanδ) of 0.0009, and a density of 1.575 mm. Broadband implementations, excessive advantage antenna styling, and occasional loss tangent produce loss because of excessive humidity is only some of the advantages of FR4 lossy collection laminate. The substrate fabric decided on layout the patch is FR4 epoxy which has a dielectric permittivity of 4.3 and the density of the substrate have to know no longer be cumbersome in order that it could be utilized in transportable gadgets and the thickness is selected to be 1.61mm. the square slotted are utilized in layout to lower the mirrored image coefficient and growth the impedance matching and efficiency. The designed antenna is (39.85 ×36.70 ×1.575mm3) The shape of rectangular patch is proven in fig 1.

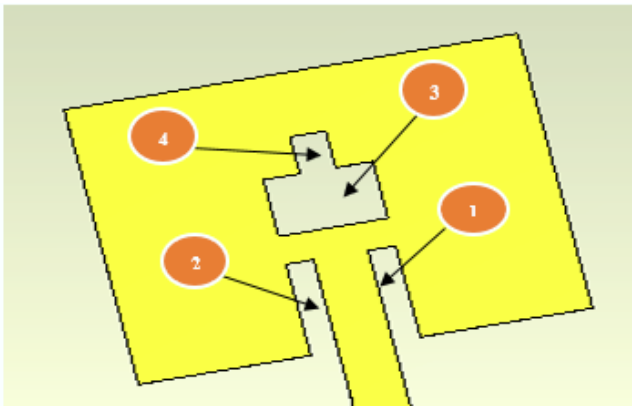

Fig. 1. Shape Rectangular Patch.

TABLE I. ANTANNA HOLES SIZES

Number	X min	X max	Y min	Y max	Z min	Z max
1	25.53	27.06	20.45	26.89	1.575	1.61
2	20.94	22.47	20.45	26.89	1.575	1.61
3	20.94	27.07	28.85	32.85	1.575	1.61
4	23.0	25.0	32.55	35.45	1.575	1.61

A. Simulation outcome.

Microstrip patch become explained and simulated usage of the present-day model for CST to take a look at the overall achievement parameters of the radiating patch element. The device has validated to have higher reliability and accuracy to assess the antenna layout parameters which includes mirrored image coefficient, efficiency, gain, creativity, radiated power, powerful angle, etc. The width and duration of the proposed antenna to be operated at 3.5GHz Here we're taking FR4 lossy dielectric cloth which has a dielectric consistent of 4.3 and top of substrate is taken as 1.61 mm. The Operating Frequency of the antenna is 3.5 GHz, which is chosen for WIMAX applications. By those parameters we will calculate the duration (L), Width (W) of patch easily.

B. S-Parameter

The S11 defines the energy transmitted from port one to port one itself, for this reason defining the mirrored image withinside the antenna. For most radiation, the mirrored image has to be as much less as feasible to make the antenna extra efficient. S11 parameter decrease than -20 dB with a value of -26.523 dB on the ringing recurrence 3.5 GHz.

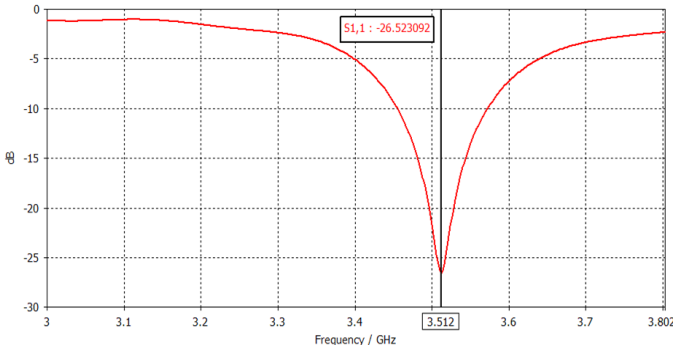

Fig. 2. S11 Simulated Parameter curve.

C. VSWR

The value of the return loss of - 26,523 dB with the bandwidth obtained at 120.5 MHz. While in Fig 3 obtained VSWR at 1.099, which means that the antenna can radiate almost all power flowed and little power is reflected back from the antenna.

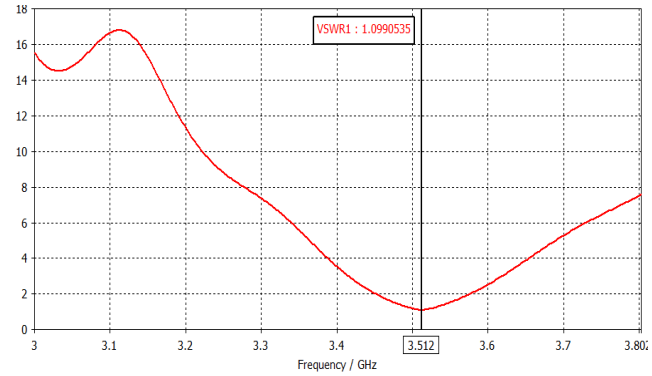

Fig. 3. Voltage Standing Wave Ratio simulation.

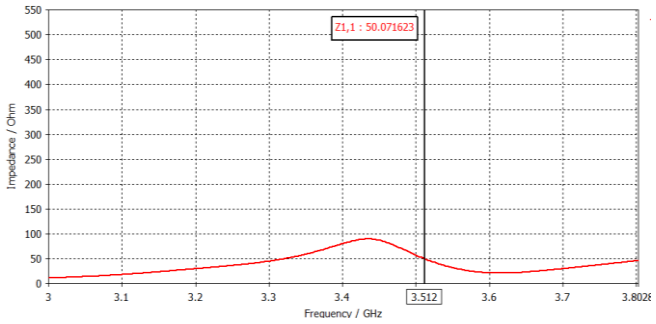

Fig. 4. Z11 Impedance simulation.

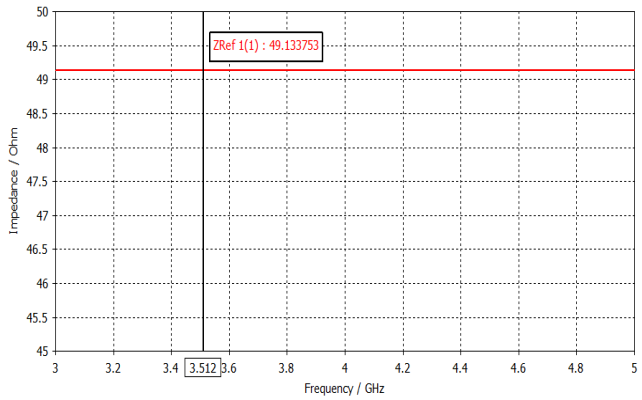

Fig. 5. Z Ref Impedance simulation.

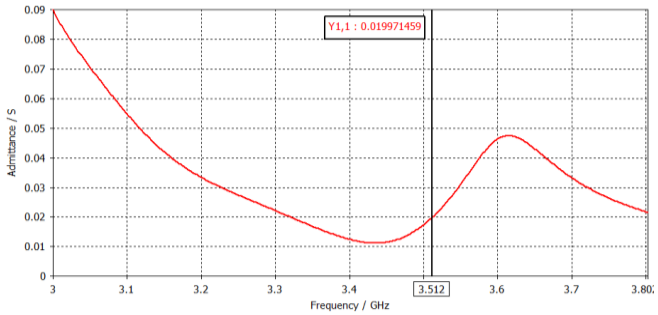

Fig. 6. Y Parameters simulation.

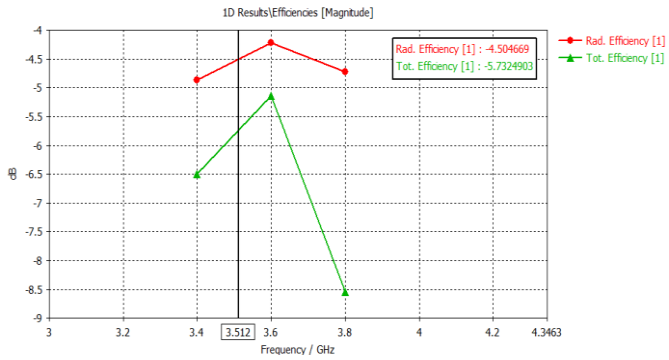

Fig. 7. radiated and total Efficiency simulation.

The following figure shows radiation pattern in fig 8,9,10 and fig 11.

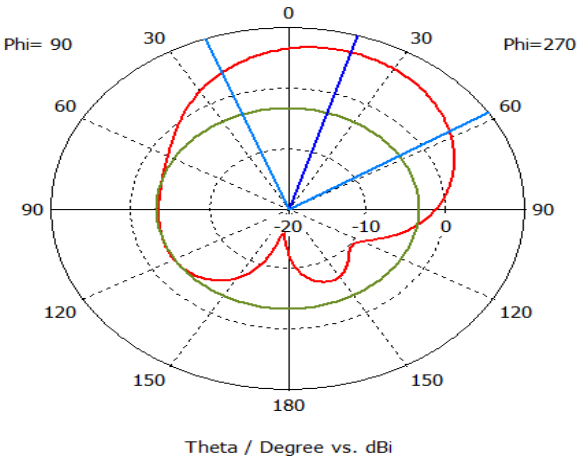

Fig. 8. Antenna radiation pattern to Phi= 270 at 3.5 GHz

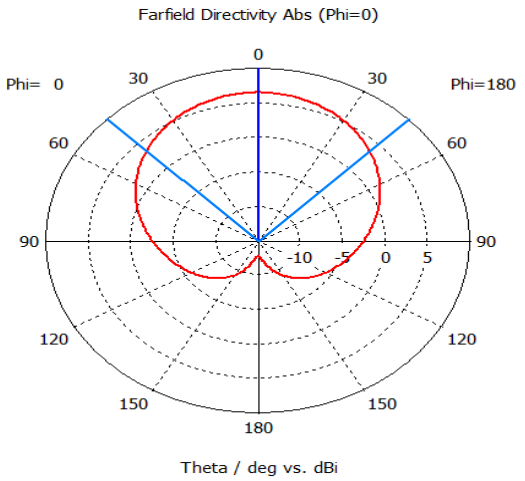

Fig. 9. Antenna radiation pattern to Phi=0 at 3.5 GHz.

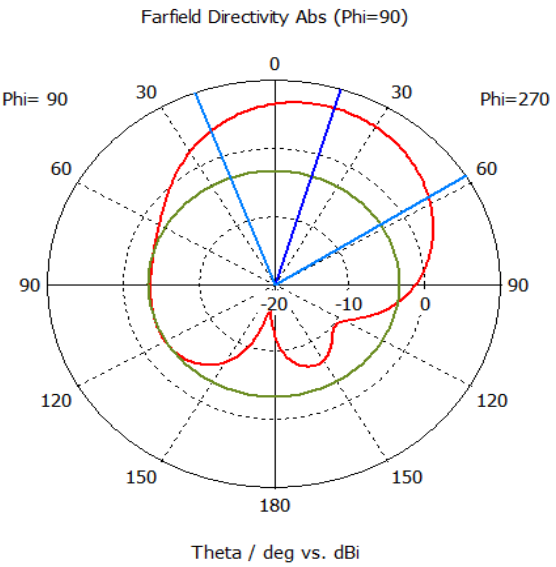

Fig. 10. Antenna radiation pattern to Phi=90 at 3.5 GHz.

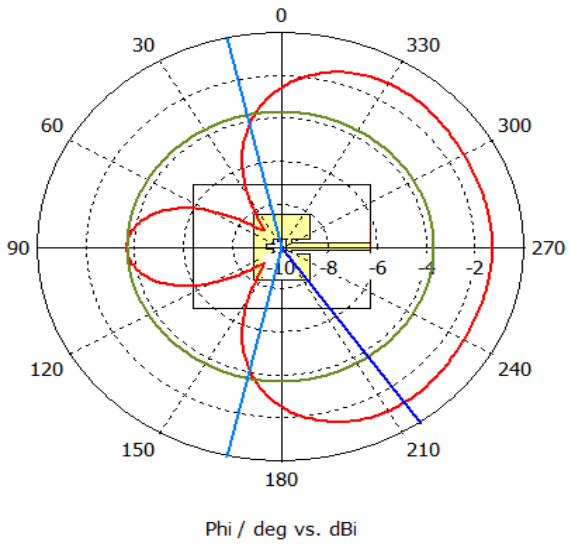

Fig. 11. The radiation pattern of antenna Phi vs deg. dBi at 3.5 GHz.

III. SURFACE CURRENT DISTRIBUTION

Antenna surface current simulation shows in fig 12.

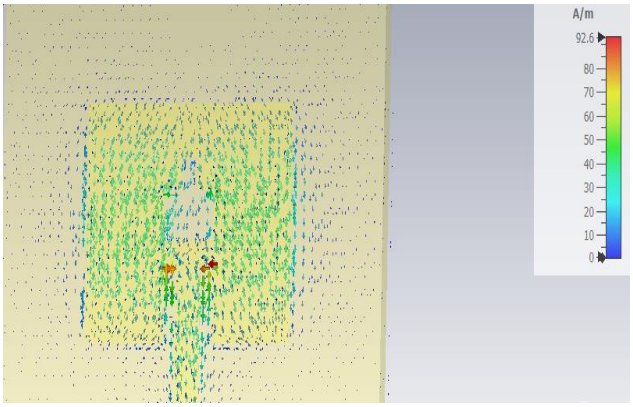

Fig. 12. surface current simulation.

A. *Gain*

Antenna Gain is likewise referred as Power advantage or clearly gain. This combines of antenna performance and creativity. The advantage acquired with inside the antenna simulation process. Advantage on the center frequency of 3.5 GHz at 7.07 dBi. For a transmitting antenna, it suggests how efficaciously the antenna is capable to radiate the given energy into an area in a selected direction. While in case of receiving antenna, it suggests how nicely the antenna is to transform the obtained electromagnetic waves into electric energy. as well in figure 11 and 12 shows the gain in the antenna process simulation, the gain at the middle frequency of 3.5 GHz at 7.07dBi.

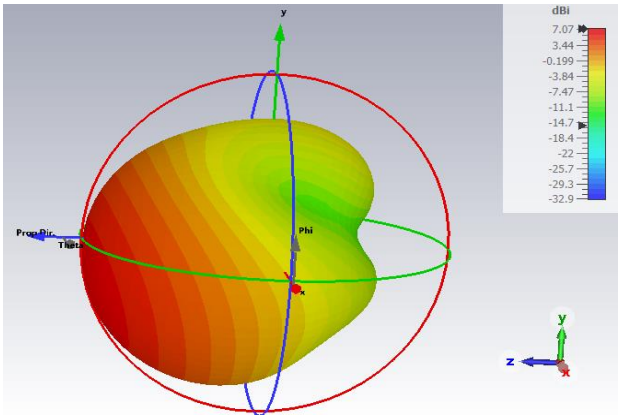

Fig. 13. 3-D radiation pattern of antenna Simulation Results.

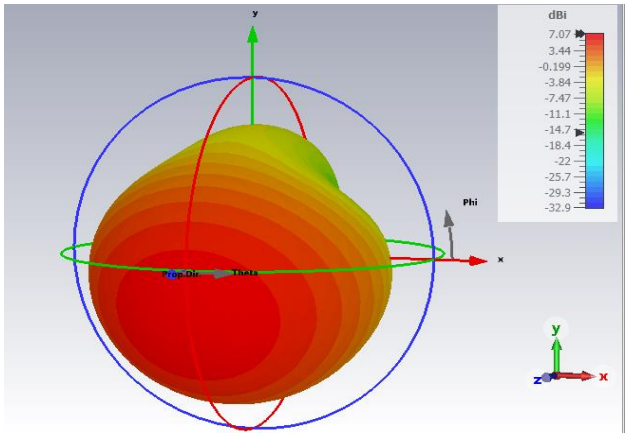

Fig. 14. 3-D radiation pattern and gain.

CONCLUSION

The analysis paper conferred the planning and simulation of the oblong patch antenna at 3.5 megacycle per second this state of labor includes the design procedure of the micros trip patch at a ringing recurrence of 3.51 GHz. It will turn out an antenna with a comeback loss of -26,523 and a VSWR of 1.0990. However, the parameters are thought of well enough, because it is glad of the specified parameters. It's as a result of the information measure decreased. The VSWR, return loss, and gain are satisfied the desired parameters. Also, the bandwidth satisfies the bandwidth for 5G a minimum of one hundred and twenty-one MHz Finally, the simulation results show that the antenna is in accordance with the specified parameters. The antenna is helpful for 5G applications. The results show the improved bandwidth, the gain is high and also the s parameters graphical results show the rise within the potency and wide radiation patterns elaborated experimental studies will be concerned at a later stage to seek out a style procedure for balanced amplifying antennas.

CONTRUBITION OF THE AUTHORS

The contributions of the authors to the article are equal.

CONFLICT OF INTEREST

There is no conflict of interest between the authors.

STATEMENT OF RESEARCH AND PUBLICATION ETHICS

Research and publication ethics were observed in this study

REFERENCES

[1] C. Singh and G. Kumawat, "A compact rectangular ultra-wideband microstrip patch antenna with double band notch feature at Wi-Max and WLAN," *Wireless Personal Communications*, vol. 114, no. 3, pp. 2063-2077, 2020.

[2] K. Prabha, B. Nataraj, and M. Jagadeeswari, "Design and Analysis of Microstrip Patch Antenna for Sub-6GHz Applications," in *2022 First International Conference on Electrical, Electronics, Information and Communication Technologies (ICEEICT)*, 2022: IEEE, pp. 1-3.

[3] N. Ramli, S. K. Noor, T. Khalifa, and N. Abd Rahman, "Design and performance analysis of different dielectric substrate based microstrip patch antenna for 5G applications," *Design and Performance*, vol. 11, no. 8, 2020.

[4] A. A. Abdulbari *et al.*, "Design compact microstrap patch antenna with T-shaped 5G application," *Bulletin of Electrical Engineering and Informatics*, vol. 10, no. 4, pp. 2072-2078, 2021.

[5] J. B. Ramek and Y. S. Khee, "The Effect of Magneto Dielectric Material to the Performance of Rectangular Microstrip Patch Antenna," *Evolution in Electrical and Electronic Engineering*, vol. 2, no. 2, pp. 436-443, 2021.

[6] S. K. Ibrahim and Z. T. Jebur, "A High Gain Compact Rectangular Patch Antenna For 5G Applications," in *2021 International Conference on Communication & Information Technology (ICICT)*, 2021: IEEE, pp. 156-160.

[7] R. H. Thaher and Z. S. Jamel, "New design of dual-band microstrip antenna for Wi-Max and WLAN applications," in *2018 1st International Scientific Conference of Engineering Sciences-3rd Scientific Conference of Engineering Science (ISCES)*, 2018: IEEE, pp. 131-134.

[8] F. Z. Moussa, S. Ferouani, Y. Belhadef, and G. Abdellaoui, "New design of miniature rectangular patch antenna with DGS for 5G mobile communications," in *2021 International Conference on Information Systems and Advanced Technologies (ICISAT)*, 2021: IEEE, pp. 1-5.

[9] D. Paragya and H. Siswono, "3.5 GHz rectangular patch microstrip antenna with defected ground structure for 5G," *ELKOMIKA: Jurnal Teknik Energi Elektrik, Teknik Telekomunikasi, & Teknik Elektronika*, vol. 8, no. 1, p. 31, 2020.

[10] S. Sekkal, L. Canale, and A. Asselman, "Flexible textile antenna design with transparent conductive fabric integrated in OLED for WiMAX

wireless communication systems," in *2020 IEEE International Conference on Environment and Electrical Engineering and 2020 IEEE Industrial and Commercial Power Systems Europe (EEEIC/I&CPS Europe)*, 2020: IEEE, pp. 1-4.

Simulation of Rectangular Microstrip Antennas and the Effect of Variable Frequencies and Performance Analysis

Received: 18 December 2022; Accepted: 19 December 2022 *Research Article*

Waled Mohammed M. Aburas
Electrical and electronics engineering
Karabuk University
Karabuk, Turkey
waled.aburas2018@gmail.com

***Abstract* -The analysis paper is predicated on the study of appropriate Simulation of microstrip antennas for 5G technology for the utilization of telecommunication applications. Mobile users want a lot of options on their mobile phones akin to high knowledge rate, economical telecommunication, and luxury to use varied applications. The antennas' carrying out in terms of reflection coefficient, (VSWR), bandwidth, gain, and efficiency performance are simulated four designs assumed, and compared using Studio Suite Antenna magus (CST, 2021). technology provides very high bandwidth, reduced latency better Quality of Service, this rectangular microstrip patch antenna is used in this Simulation because it is a basic antenna and easy to design, we utilized FR4-Generic substrate material with varying relative permittivity has been designed, the other hand, optimum capacity, and a wide band of spectrum availability furthermore demand to occur for mobile telecommunication. we utilized Simulation of various frequencies 4.8 GHz5.8 GHz, 6.4 GHz and 7.2 GHz. However, these four designs patch antenna dimensions were slightly different from each other.in addition, we analyze the effect of variable frequencies and Performance Analysis, also analysis of various dimensions of an antenna. The impedance ratings were slightly higher, respectively, and gain it was accepted,7.219 dbi,7.233dbi,7.227dbi, and 7.252dbi, also VSWR 1.017, are as well considered which is examine whether the microstrip patch antenna design is appropriate for 5G.**

***Keywords* --Microstrip antenna, rectangular patch antenna, Efficiency, gain,5G**

I. INTRODUCTION

Microstrip patch antennas (MSPA) are becoming more popular in wireless applications due to their low-profile design. built-in antennas in portable wireless devices such as mobile phones and communication antennas on missiles. Because they must be tiny and conformal. One of the challenging issues is to design compact, high-performance, and wideband antennas. In moving toward to fifth-generation (5G) network, many studies have been conducted on (MSPA) that are because of their compactness, cheap and fast manufacturing. The attenuation of the materialistic dimension of an antenna implies a harmonic increase frequency. the main idea of miniaturization is to shift the resonance to lower frequencies to reap an electrically small antenna. the layout of the antenna had visible a vast project due to the speedy development in (WiMAX) and communique structures. Patch antenna designs had demonstrated because the first-class option to be utilized in wireless communique gadgets with many advantages which includes light-weight, planar shape, small size, low profile, and compatibility with microwave integrated circuits (MICs). also, concerning international Interoperability for Microwave access (WiMAX) in this survey, we utilized FR4-Generic substrates materials with varying relative permittivity has been designed in this antenna the substrate thickness it same 1.10 mm and by calculating the area of each antenna, the following became clear sloped down as the frequency increases, the area decreases from 286.99mm2 in frequency 4.8 GHz to 130.57mm2 in frequency 7.2GHz respectively under different frequencies , 4.8 GHz,5.8 GHz 6.4 GHz, and 7.2 GHz. The dimensions of this patch antenna were slightly different from each other. In addition, we analyze the effect of variable frequencies and performance analysis, as well as measurements of various parameters of the antenna design. The impedance ratings were slightly higher, respectively, and the gain, 7.219 dBm, 7.233 dBm, 7.227 dBm, and 7.252 dBm, also VSWR 1.017, 1.074,1.072,1.049 was accepted and checked It grew to become out the microstrip patch antenna layout is appropriate for a 5G network.

II. PROPOSED RECTANGULAR ANTENNA

The goal is to own a high advantage and performance to make sure that the foremost records switches in any wireless communication devices space antenna are the amount one requirement. once birth out any microstrip patch antenna, several improvement ways are used, and twin feed. Wide information measure antennas are applied for a huge type of community frequencies, that are larger and inexperienced for a few distance space implementations. section distinction is simple to maintain the foremost common issue in wireless communication devices is the orientation of receivers and transmitters. Multiband operation and antenna length miniaturization could also be performed by utilizing the noted options of self-similarity and area filling.

The important three layout parameters of the antenna are the ringing recurrence (fr), the relative permittivity of the substrate (Er), and the density of the substrate (h). The ringing recurrence of the antenna needs to be appropriate for the WiMAX. In these four designs, the parameters' different frequencies are 4.8 GHz,5.8 GHz 6.4 GHz, and 7.2 GHz, also substrate (Er) 4.35, substrate (h) 1.10mm, a loss tangent (tanδ) of 0.00013.

Microstrip patches become explained and simulated usage of the present-day model for Studio Suite Antenna magus (CST, 2021). to take a look at the overall achievement parameters of the radiating patch element. The device has been validated to have higher reliability and accuracy to assess

the antenna layout parameters which include mirrored image coefficient, efficiency, gain, creativity, radiated power, powerful angle, etc. The width and duration of the proposed antenna to be operated are different frequencies 4.8GHz.5.8GHz,6.4GHz, and 7.2GHz Here we're taking FR4-Generic dielectric cloth which has a dielectric consistency of (Er) 4.35, and the top of high substrate (h)is taken as 1.15 mm,1.05mm,0.95mm,0.90mm The Operating different Frequency of the antenna is chosen for WIMAX applications.

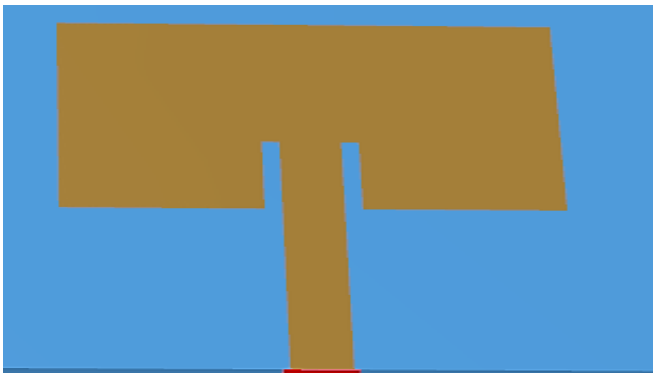

Fig. 1. Shape Rectangular Patch.

TABLE I. ANTENNA DESIGN PARAMETERS

Frequency	substrates material	substrate (h)	patch area W×L	Feed line area WF×LF
4.8 GHz	FR4-Generic	1.15 *mm*	286.99 mm^2	2.217×17.20 *mm*
5.8 GHz	FR4-Generic	1.05 *mm*	198.35 mm^2	2.025×14.23 *mm*
6.4 GHz	FR4-Generic	0.95 *mm*	163.26 mm^2	1.832×12.90 *mm*
7.2 GHz	FR4-Generic	0.90 *mm*	130.57 mm^2	1.639×11.46 *mm*

III. SIMULATION OUTCOME

The four antennas layout for the (MSPA) was analyzed and simulated utilizing of the Studio Suite Antenna magus (CST, 2021) To examine the overall performance parameters of the various designed antennas. This device has tested to have higher reliability and accuracy to assess the antenna layout parameters inclusive of mirrored image coefficient, efficiency, gain, directivity, radiated power, powerful angle, etc., The width and period of the proposed antenna to be operated at many frequencies It turned into referred to formerly are located the use of the analytical expression given through the above-referred to equations.

A. Antenna Performance Parameters

Radiation efficiency, which indicates or mensuration the amounts of the losses in the antenna, is definite as the percent or ratio of radiated power (Pr) from the patch antenna to input power (Pi) for the same antenna. The input power (Pi) is converted to radiant power, surface wave energy, and a small fraction dissipated due to dielectric losses and conductors. Another important parameter of an antenna it contains much data that is significant in the design is the bandwidth, in general principle, most of the time, the impedance matching or return loss bandwidth is identified to measure the antenna bandwidth. it is equal to 960 MHz,1.16 GHz, 1.28 GHz, and 1.44 GHz, also expressed by percent %, We also explain some other outputs frequency values at minimum VSWR, Max gains, and Impedance Imaginary As shown in the following table No.2.

TABLE II. ANTENNA PERFORMANCE PARAMETERS

Frequency	4.8 GHz	5.8 GHz	6.4 GHz	7.2 GHz
VSWR	1.017	1.074	1.072	1.049
Frequency value at minimum VSWR	4.748 GHz	5.740 GHz	6.333 GHz	7.116 GHz
BW	960 MHz	1.16 GHz	1.28 GHz	1.44 GHz
BW below 2.0 level	78.73 MHz	108.8 MHz	119.9 MHz	135.4 MHz
Impedance Imaginary	52 Ω	53 Ω	53.6 Ω	54 Ω
Max gain	7.219 dBi	7.233 dBi	7.227 dBi	7.252 dBi
minimum S parameter value	-41.34 dB	-28.92 dB	-29.18 dB	-32.36 dB
Frequency value at minimum S parameter	4.768 GHz	5.760 GHz	6.355 GHz	7.156 GHz
Beamwidth (a above 10.0 dB below peak level) ϕ= 0° & ϕ= 90°	77.77° & 90.18°	77.12° & 90.61°	77.08° & 90.61°	76.11° & 90.44°

B. S Parameters

The S11 defines the energy transmitted from port one to port one itself, for this reason defining the mirrored image withinside the antenna.

For most radiation, the mirrored image has to be as much less feasible to make the antenna extra efficient. The S11 parameter decreased to -20 dB with a value of -41.43 dB on the ringing recurrence of 4.8 GHz, -28.92 dB on the ringing recurrence of 5.8 GHz, -29.18 dB on the ringing recurrence of 6.4 GHz, finally -32.36 dB on the ringing recurrence 7.2 GHz.

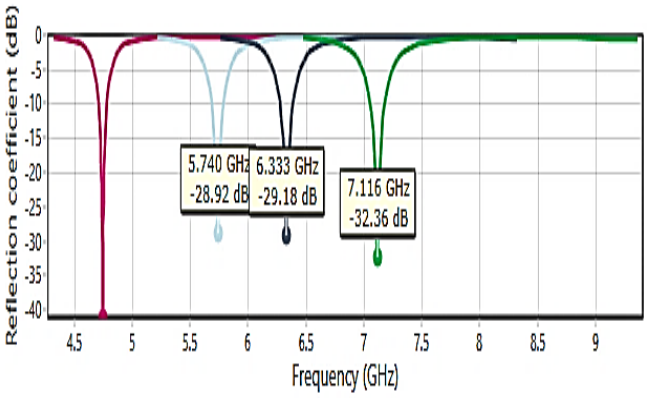

Fig. 2. minimum S parameters(S11)

C. VSWR

Additionally, the excellent significance parameter of an antenna is the reflection coefficient of the antenna inputs. It is

definite as the ratio of the reflected current (Ir) or voltage (Vr) to the incident current (Ii) or voltage (Vi), as in S11, where the patch antenna is an analyzer. It is the measure of the impedance of a failure to correspond (mismatch) between the antenna input and the feed source. The unit of measurement of mismatch is usually described in terms of a return loss S11 or voltage standing wave ratio (VSWR), And after comparing the results, it becomes clear that they are all acceptable, with a preference for frequency 4.8 GHz which equals 1.017 as shown in the figures.

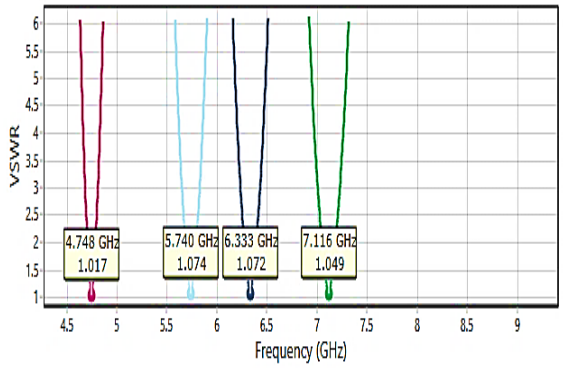

Fig. 3. Voltage Standing Wave Ratio simulation

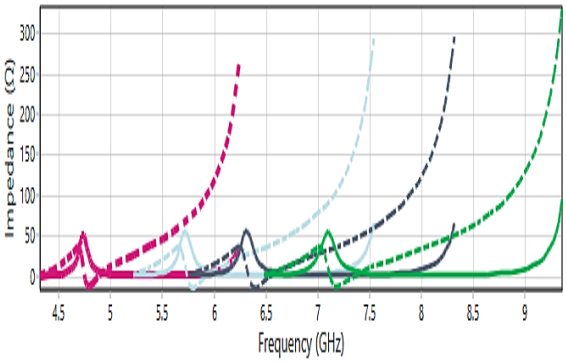

Fig. 4. the average impedance value of data

D. TOTAL GAIN

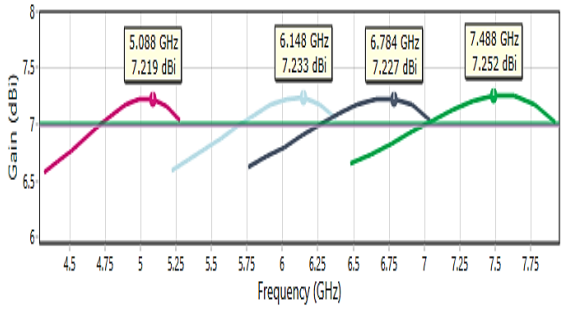

Fig. 5. the average gain value and frequency maximum gain value of data

E. SMITH CHART

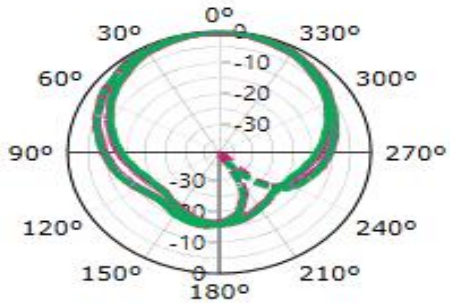

Fig. 6. maximum gain value when $\emptyset = 0^{\circ}$ *and* $\emptyset = 90^{\circ}$

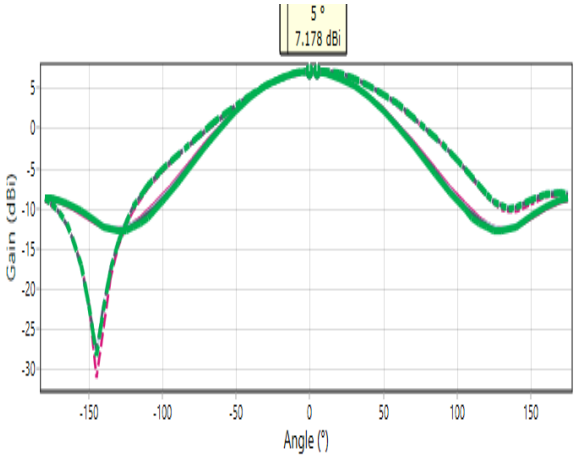

Fig. 7. maximum gain value when $\emptyset = 0^{\circ}$ *and* $\emptyset = 90^{\circ}$

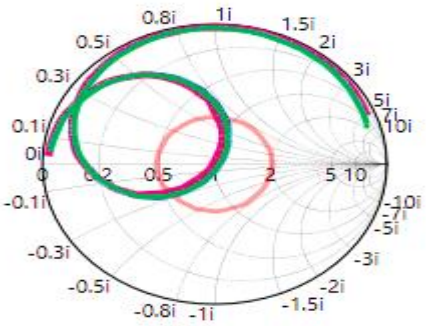

Fig. 8. input impedance smith chart

F. 3D GAIN radiation pattern

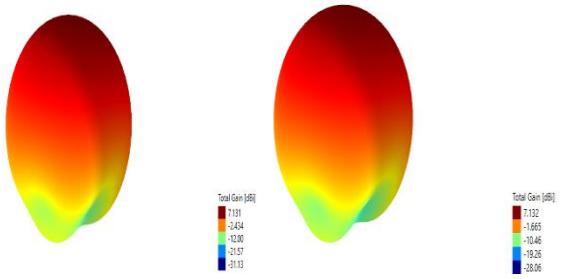

Fig. 9. 3-D radiation pattern of antenna Simulation Results 4.6 GHz, and 5.8 GHz.

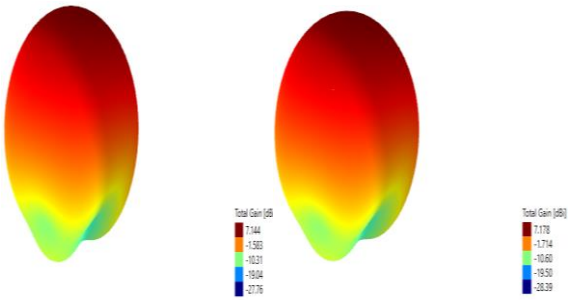

Fig. 10. 3-D radiation pattern of antenna Simulation Results 6.4 GHz and 7.2 GHz.

CONCLUSION

In this study, A rectangular (MSA) has been proposed for 5G packages in reaction to the developing call for cellular data and cellular devices. with designs of four patch antennas with four different frequencies This antenna has a resonance frequency of 4.8 GHz,5.8 GHz, 6.4 GHz, and 7.2 GHz for which VSWR respectively equals 1.017,1.074. 1.072 and 1.049. also, the bandwidth respectively equals 960MHz, 1.16 GHz, 1.28 GHz, and 1.44 GHz (relative operational band 20%), and the average gain value is approximately 7.23 dBi. the data shows that with the diversity of frequency the antennas carry out well.

CONTRUBITION OF THE AUTHORS

The contributions of the authors to the article are equal.

CONFLICT OF INTEREST

There is no conflict of interest between the authors.

STATEMENT OF RESEARCH AND PUBLICATION ETHICS

Research and publication ethics were observed in this study

REFERENCES

[1] D. Tiwari, J. A. Ansari, A. K. Saroj, and M. Kumar, "Analysis of a Miniaturized Hexagonal Sierpinski Gasket fractal microstrip antenna for modern wireless communications," *AEU-International Journal of Electronics and Communications*, vol. 123, p. 153288, 2020.

[2] A. H. Mahmud and A. Roy, "Bandwidth Enhancement of a Microstrip Patch Antenna for 5G Applications," Department of Electronic and Telecommunication Engineering, 2022.

[3] A. E. Almuzwghi and L. Brian, "Broad band microstrip patch antenna based on foam-filled and one open slot on backward of radiating layer," *Journal of Computer and Communications*, vol. 7, no. 06, p. 15, 2019.

[4] R. Przesmycki, M. Bugaj, and L. Nowosielski, "Broadband microstrip antenna for 5G wireless systems operating at 28 GHz," *Electronics*, vol. 10, no. 1, p. 1, 2020.

[5] M. T. GÜNEŞER and C. ŞEKER, "Compact microstrip antenna design for 5G communication in millimeter wave at 28 GHz," *Erzincan University Journal of Science and Technology*, vol. 12, no. 2, pp. 679-686.

[6] C. Singh and G. Kumawat, "A compact rectangular ultra-wideband microstrip patch antenna with double band notch feature at Wi-Max and WLAN," *Wireless Personal Communications*, vol. 114, no. 3, pp. 2063-2077, 2020.

[7] S. Sadasivam, V. T. Bai, R. Yuvaraj, P. Rahul, and M. R. Thomas, "Comparison of FR4 and Roger substrates in multiband two-slot rectangular patch antenna for 5G applications," *Materials Today: Proceedings*, vol. 55, pp. 452-454, 2022.

[8] K. Prabha, B. Nataraj, and M. Jagadeeswari, "Design and Analysis of Microstrip Patch Antenna for Sub-6GHz Applications," in *2022 First International Conference on Electrical, Electronics, Information and Communication Technologies (ICEEICT)*, 2022: IEEE, pp. 1-3.

[9] N. Ramli, S. K. Noor, T. Khalifa, and N. Abd Rahman, "Design and performance analysis of different dielectric substrate based microstrip patch antenna for 5G applications," *International Journal of Advanced Computer Science and Applications*, vol. 11, no. 8, 2020.

[10] E. Chemweno, P. Kumar, and T. Afullo, "Design of high-gain wideband substrate integrated waveguide dielectric resonator antenna for D-band applications," *Optik*, p. 170261, 2022.

[11] S. A. Hafeez and M. Sathesh, "Design of Novel Rectangular Patch Microstrip Antenna for Ku Band Applications and Comparison of Gain with Circular Patch Antenna," in *2022 2nd International Conference on Innovative Practices in Technology and Management (ICIPTM)*, 2022, vol. 2: IEEE, pp. 594-599.

[12] J. B. Ramek and Y. S. Khee, "The Effect of Magneto Dielectric Material to the Performance of Rectangular Microstrip Patch Antenna," *Evolution in Electrical and Electronic Engineering*, vol. 2, no. 2, pp. 436-443, 2021.

[13] S. K. Ibrahim and Z. T. Jebur, "A High Gain Compact Rectangular Patch Antenna For 5G Applications," in *2021 International Conference on Communication & Information Technology (ICICT)*, 2021: IEEE, pp. 156-160.

[14] M. Z. B. Chowdhury, M. T. Islam, H. Rmili, I. Hossain, M. Z. Mahmud, and M. Samsuzzaman, "A low-profile rectangular slot antenna for sub-6 GHz 5G wireless applications," *International Journal of Communication Systems*, vol. 35, no. 17, p. e5321, 2022.

[15] R. Bancroft, "Microstrip Antenna Efficiency and Surface Wave Loss," *IEEE Transactions on Antennas and Propagation*, vol. 69, no. 8, pp. 5032-5035, 2021.

[16] S. K. Ezzulddin, S. O. Hasan, and M. M. Ameen, "Microstrip patch antenna design, simulation and fabrication for 5G applications," *Simulation Modelling Practice and Theory*, vol. 116, p. 102497, 2022.

[17] J. Huang, X. Li, and Y. Li, "A Millimeter-wave Microstrip MIMO Antenna for n260 Frequency-band," in *2021 International Conference on Microwave and Millimeter Wave Technology (ICMMT)*, 2021: IEEE, pp. 1-3.

[18] F. Z. Moussa, S. Ferouani, Y. Belhadef, and G. Abdellaoui, "New design of miniature rectangular patch antenna with DGS for 5G mobile communications," in *2021 International Conference on Information Systems and Advanced Technologies (ICISAT)*, 2021: IEEE, pp. 1-5.